Global and Planetary Change 76 (2011) 33–55

Contents lists available at ScienceDirect

Global and Planetary Change

journal homepage: www.elsevier.com/locate/gloplacha

Sediment provenance, reworking and transport processes in the Indus River by U–Pb dating of detrital zircon grains

Anwar Alizai [a,*], Andrew Carter [b], Peter D. Clift [a], Sam VanLaningham [c], Jeremy C. Williams [e], Ravindra Kumar [d]

[a] School of Geosciences, University of Aberdeen, Meston Building, Aberdeen, AB24 3UE, UK
[b] Department of Earth and Planetary Sciences, Birkbeck College, Malet Street, London, WC1E 7HX, UK
[c] School of Fisheries and Ocean Sciences, University of Alaska Fairbanks, Fairbanks, AK 99775-7220, USA
[d] Department of Environmental, Earth and Ocean Sciences, University of Massachusetts-Boston, Boston, MA 02125, USA
[e] 342 Clover Water Gardens, Kalyani Nagar, Pune 411006, Maharashtra, India

ARTICLE INFO

Article history:
Received 29 April 2010
Accepted 29 November 2010
Available online 9 December 2010

Keywords:
erosion
zircon
climate
provenance

ABSTRACT

We present new major and trace element data, together with U–Pb ages for zircon sand grains from the major tributaries of the Indus River, as well as the adjacent Ghaggar and Yamuna Rivers and from bedrocks within the Sutlej Valley, in order to constrain the origin of the sediment reaching the Arabian Sea. Zircon grains from the upper Indus are generally younger than 200 Ma and contrast with those from the eastern tributaries eroded from Himalayan sources. Grains younger than 15 Ma, which typify the Nanga Parbat Massif, comprise no more than 1–2% of the total, even in the upper Indus, showing that this terrain is not a major sediment producer, in contrast with the Namche Barwe Massif in the eastern Himalayan syntaxis. The Sutlej and Yamuna Rivers in particular are very rich in Lesser Himalayan-derived 1500–2300 Ma zircons, while the Chenab is dominated by 750–1250 Ma zircons, mostly eroded from the Greater Himalaya. The upper Indus, Chenab and Ravi yield zircon populations broadly consistent with the outcrop areas, but the Jhelum and the Sutlej contain many more 1500–2300 Ma zircons than would be predicted from the area of Lesser Himalayan rock within their drainages. A significant population of grains younger than 200 Ma in the sands of the Thar Desert indicates preferential eolian, monsoon-related transport from the Indus lower reaches, rather than reworking from the local rivers. Modelling of observed zircon ages close to the delta contrasts with modern water discharge. The delta is rich in zircons dating 1500–2300 Ma, while discharge from modern rivers carrying such grains is low. The modest size of the Sutlej, the richest source of these materials in the modern system, raises the possibility that the compositionally similar Yamuna used to flow westwards in the recent past. Our data indicate a non-steady state river with zircon transport times of 5–10 k.y. inferred from earlier zircon dating of delta sands. The modern delta zircons image an earlier, likely Early-Mid Holocene, erosional state, in which the Lesser Himalaya were more important as sediment suppliers. Early-Mid Holocene sands show much less erosion from the Karakoram–Transhimalaya compared to those deposited at the Last Glacial Maximum, or calculated from the modern discharge. We favour variations in summer monsoon intensity as the primary cause of these temporal changes.

1. Introduction

Fluvial systems are particularly sensitive to climatic and tectonic change (e.g., Métivier and Gaudemer, 1999; Whipple, 2001). Erosion by rivers records changes in Earth surface and solid Earth processes, mainly through deposited sediment volumes and thicknesses (i.e., rates and fluxes), the morphology of the fluvial system, and the sediment composition, which reveals information about source areas of sediment (i.e., provenance). Whereas difficulties arise in determining rates and fluxes of sediment in rivers (Syvitski, 2003), compositional analysis of fluvial sediments for provenance provides a fairly rapid, accessible methodology to investigate changes in erosion both in modern and palaeo-fluvial settings, and thus places relative constraints on river discharge, sediment flux, and spatial patterns in the focus of erosion.

The Indus River system of Pakistan and western India has experienced large changes to its fluvial system throughout geologic time, both as a result of tectonically driven drainage reorganization (Clift and Blusztajn, 2005) and in response to climate, in particular the South Asian Monsoon. During the Holocene the Indus responded to intensification of the summer Monsoon from 14 to 8 ka by preferentially eroding the Lesser Himalayas, as expressed through

* Corresponding author.
E-mail address: a.alizai@abdn.ac.uk (A. Alizai).

0921-8181/$ – see front matter © 2010 Elsevier B.V. All rights reserved.
doi:10.1016/j.gloplacha.2010.11.008

single grain mica Ar–Ar, zircon U–Pb ages, and bulk sediment Nd isotopic data (Clift et al., 2008a). However, although there were reasonably good documentation of the source rock compositions, the actual material now coming from each of the Indus River tributaries was not well constrained. In this paper, we address our poor understanding of the major Indus tributaries by providing new U–Pb zircon ages from each of the five modern tributaries (Jhelum, Chenab, Ravi, Beas and Sutlej), as well as the neighbouring Ghaggar and Yamuna Rivers, in order to constrain the source of sediment to the modern Indus River and thus to determine where erosion is now most active in the western Himalaya.

The Indus basin spans areas of strong climate-tectonic forcing (e.g., Nanga Parbat; Fig. 1) and has a strong, erosive monsoonal climate over parts of the drainage area (Fig. 2), which allows the relative influence of these processes in driving erosion to be compared. In addition, there is a strong gradient of rainfall across the mountains from wet in the south to the dry regions of Ladakh, the Karakoram and Tibet in the North (Fig. 2). The Indus is a sediment-productive river, which used to supply around 250 Mt/yr to the Arabian Sea prior to modern damming (Milliman and Syvitski, 1992), although estimates of the true amount range wildly from 100 to 675 Mt/yr (Ali and De Boer, 2008).

We use detrital zircon U–Pb ages in modern clastic sediments to define the origin of individual grains, and this in turn can be used to quantify erosion patterns in the modern source mountains. By defining the provenance of the sediment in the major river tributaries we also provide the tools for reconstructing palaeo-erosion patterns from old river, delta or submarine fan deposits, because the modern rivers allow us to better define the variability in source compositions available to the river. Although links have been established between modern water discharge and suspended sediment load (Ali and De Boer, 2007) the relationship between discharge and bedload is less well defined and we investigate this using the dense zircon sand grains that are largely transported in this fashion, rather than as suspended sediment. Comparison of modern discharge from the sources and the sediment now 1200 km away at the delta can further be used to assess lag times in sediment transport to the ocean.

2. Sampling strategy

Our goal was to finger-print the erosional flux from each river and by reference to the known ages of the bedrock sources within each river basin we attempt to infer which parts of the mountains are contributing most to the erosional flux from each tributary and finally to the Indus delta at the Arabian Sea. In this study we date sand grains from modern river sediments sampled from all the major catchments of the Indus system, as well as one from the neighbouring Yamuna, one from a dune in the Thar Desert in upper Punjab, and one from the ephemeral Ghaggar River, located between the Yamuna and the Sutlej (Fig. 1). We consider the Thar Desert because reworking of sands in this region may be significant at times to the composition of sands in the rivers flowing close to that region, especially the Sutlej and Ghaggar. Although, the Yamuna and the Ghaggar do not now supply the Indus delta, it has been suggested that they may have done so in the past (Ghose et al., 1979; Tripathi et al., 2004; Saini et al., 2009). As a result we finger-print these sediments so that future studies of Holocene fluvial sediments may test for their past involvement in drainage evolution.

Samples, one from each river, were taken from deposited materials within active river channels, preferably from sand bars exposed during periods of lower water discharge, or taken directly from the river in order to have confidence that the sample represented recent sediment transport. In some cases sampling occurred north of the Main Frontal Thrust (MFT) in order to avoid local contamination from

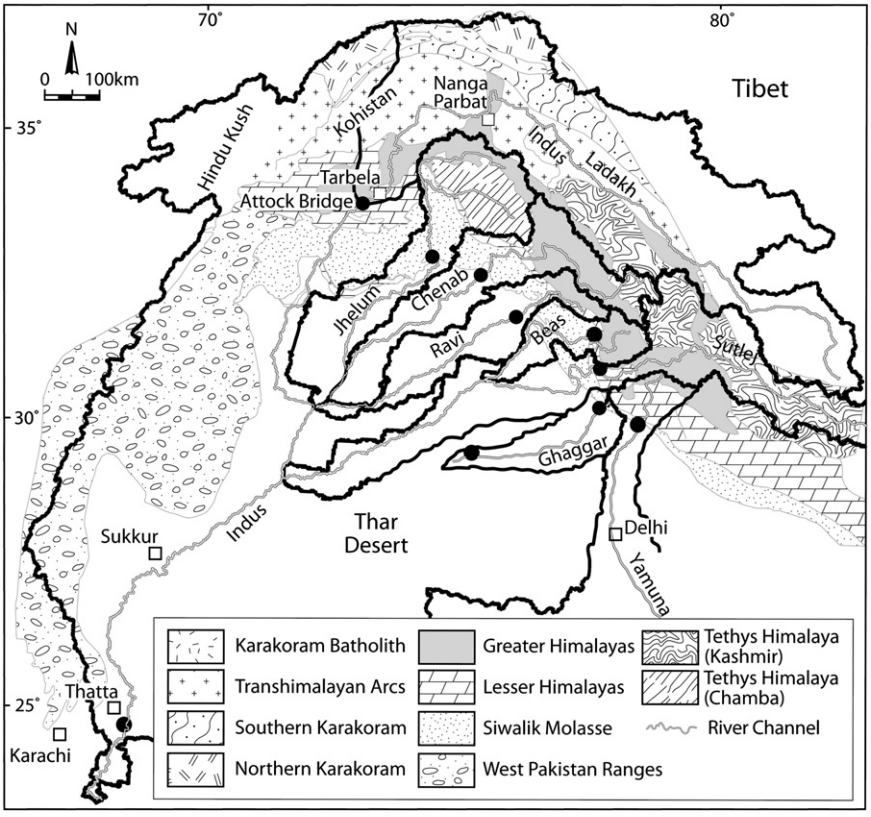

Fig. 1. Geological map of the study area showing the major tectonic units that are eroded by the Indus River and its tributaries. Map is modified after Garzanti et al. (2005). Rivers as shown in thick black lines. Sample locations are shown as filled circles. Thick black line shows the boundary of the Indus drainage, while thinner lines demark the limits of the major Himalayan tributaries.

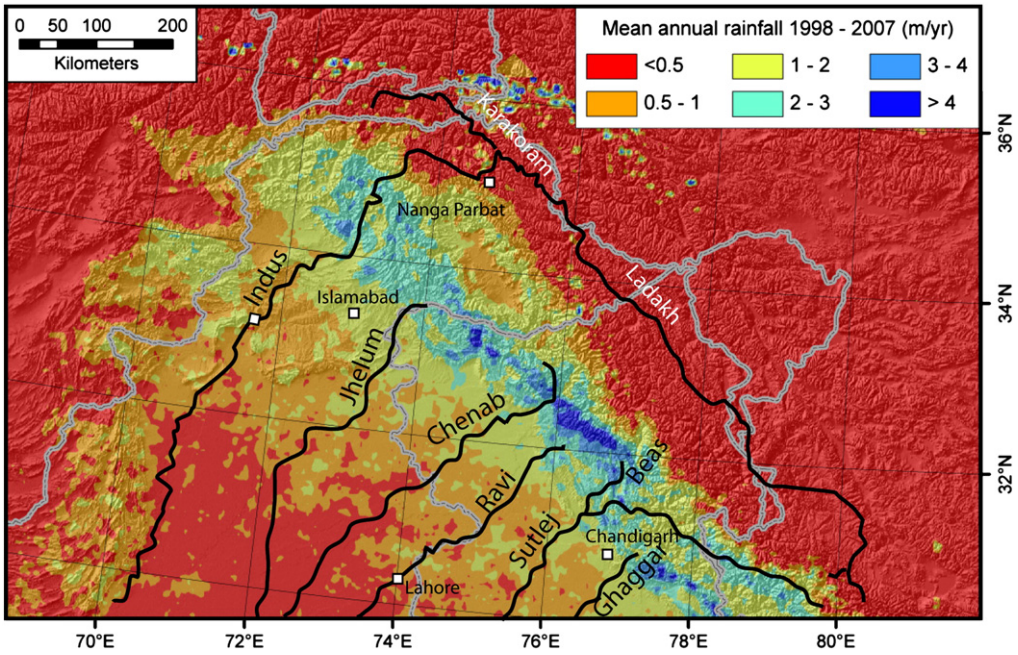

Fig. 2. TRMM rainfall map of the western Himalayan region showing mean annual rainfall across the region in relation to the river systems. The heavy rainfall in the Sutlej and Beas basins in the east is particularly noteworthy. TRMM map is unpublished from compilation of B. Bookhagen (January 2010).

reservoirs or dam construction sites, which was most disruptive in the Sutlej and Beas Rivers. This means that these samples were taken upstream of where these rivers cut the Siwaliks, and thus are unable to account for the erosional flux from these ranges, but also provide samples of the erosional flux that are not affected by this source. Because the Siwaliks do not have a unique zircon age spectrum this reduces the error in tying grains to sources in these two rivers.

In order to test the concept that fluvial detrital grains are truly representative of the bedrocks in their respective river valleys we also analyzed a number of crystalline rocks spanning the Lesser, Greater and Tethyan Himalaya along the length of the Sutlej River. We chose units that had already been the object of a structural geological study that assigned them to either Lesser or Greater Himalayan tectonic units (Vannay et al., 2004). These samples were treated in exactly the same fashion as the river sands in order to allow direct comparison of data sets.

3. Analytical approach

The U–Pb zircon analytical method was chosen because of its proven abilities to discriminate source terrains in the Himalaya, and especially in the Indus system, as a result of the significant number of existing bedrock analyses and the strong age contrasts across the western Himalaya (DeCelles et al., 2000, 2004; Clift et al., 2004; Amidon et al., 2005b; Bernet et al., 2006; Wu et al., 2007). Furthermore, although the different ranges of the western Himalaya have zircon populations that overlap with each other, each range shows a strong preferential occurrence of certain age groups. Fig. 3 shows a synthesis of U–Pb ages from the western and central Himalaya and demonstrates that zircons from the Karakoram, Transhimalaya and Nanga Parbat are always much younger than those from the Himalayan ranges. The Lesser Himalaya typically show the oldest zircon populations, with a characteristic peak at around 1850 Ma (Fig. 3D). In contrast, the rocks of the Tethyan and Greater Himalaya have a younger peak at 1000–1100 Ma, but only the Tethyan Himalaya have a resolvable peak at 500 Ma (Fig. 3B, C).

Age data from Neogene foreland sedimentary rocks of the Siwalik Group show a wide range of zircon U–Pb ages, reflecting their diverse provenance (DeCelles et al., 2004). The spread of ages from these ranges means that it is not possible to isolate their influence on the net sediment flux using zircon U–Pb ages alone. This introduces an uncertainty into attempts to deconvolve zircon populations. The Siwaliks comprise more readily erodable rock than the rest of the Himalaya and studies of Holocene terraces indicate that fluvial incision rates within the Siwaliks are the highest of any part of the range front, at least in Nepal (Lavé and Avouac, 2001). However, this same study estimated that only around 15% of the erosion was generated from the Siwaliks, while the isotopic budget of Wasson (2003) for the Ganges–Brahmaputra limited the contribution from the Siwaliks at <10% to that system. Thus, we estimate that our inability to account for the Siwaliks introduces a 10–15% uncertainty into our budget calculations, although this varies from river to river, depending on the extent of the Siwalik outcrop.

After characterizing each river sand we model how the sediment reaching the delta is mixed in order to generate the zircon populations observed in that area. In order to avoid the complication of sediment reworking in the flood plains we sampled the main rivers close to the mountain front, upstream from which there is no significant sediment storage. This assumption is of course a simplification because sediment is stored and released in terraces within the mountains. Most notably sediment may be stored in natural dams behind landslides, which are believed to be climatically modulated. Bookhagen et al. (2006) have shown that landsliding was particularly common in the Early Holocene, at least in the Sutlej Valley. Since that time the dams have been breached and the terraces are largely in a state of erosion, although their net contribution to the sediment load is much reduced compared to the Early Holocene. The degree of sediment buffering in the mountains is not well constrained, but it is likely much less than sediment storage in the foreland flood plains.

4. Methods

U–Pb ages in zircon are generally considered to reflect the time of zircon crystallization at around 750 °C (Hodges, 2003), so that they may be interpreted to record the last growth phase in a rock's history. However, zircons are known to be resistant to physical abrasion during erosion and transport, as well as to chemical weathering, making them susceptible to multiple phases of reworking (e.g.,

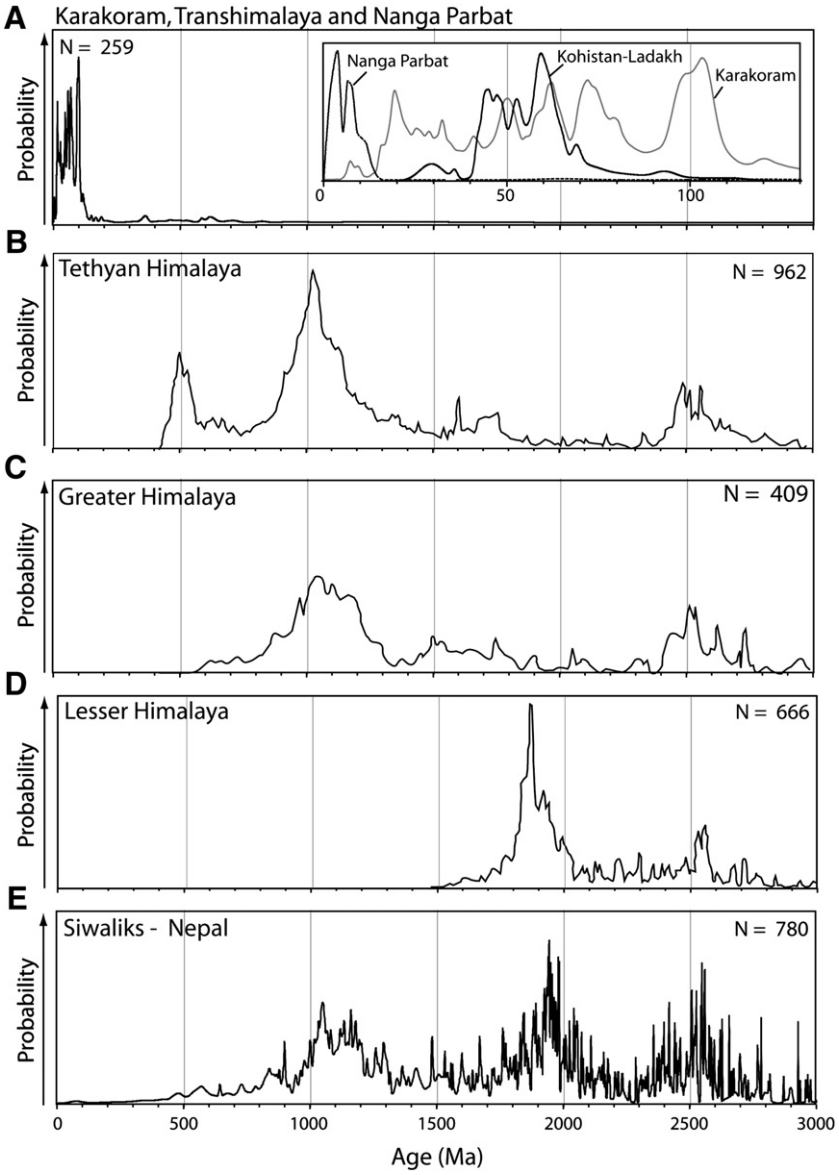

Fig. 3. Probability density plots for zircon age populations from probable source terrains within the Indus basin. Data from the Siwaliks, as well as the Tethyan, Greater and Lesser Himalaya are compiled from DeCelles et al. (2004). Karakoram data is from the compilation of Clift et al. (2004), together with more recent data from Ravikant et al. (2009). Insert in (A) shows the range of ages measured from Nanga Parbat (Zeitler and Chamberlain, 1991; Zeitler et al., 1993), the Transhimalayan Batholith (Honegger et al., 1982; Schärer et al., 1984; Krol et al., 1996; Weinberg and Dunlap, 2000; Zeilinger et al., 2001; Dunlap and Wysoczanski, 2002; Singh et al., 2007; Ravikant et al., 2009) and the Karakoram (Le Fort et al., 1983; Parrish and Tirrul, 1989; Schärer et al., 1990; Fraser et al., 2001; Ravikant et al., 2009), showing only 130 Ma in order to emphasize the differences. Note the prominent peaks <200 Ma in panel A, at ~500 and 1000 Ma in the Tethyan Himalaya (B), at ~1000 Ma in the Greater Himalaya (C), at ~1800 Ma in the Lesser Himalaya (D), and at 1100, 1900 and 2500 Ma in the Siwaliks (E).

DeCelles et al., 2000, 2004; Campbell et al., 2005). Although it is impossible to say precisely where a given grain is derived from, it is possible to suggest the most likely source rock unit for many grains, making U–Pb dating a powerful provenance tool in this area.

U–Pb dating analyses were performed on polished grain mounts by laser ablation-inductively coupled plasma mass spectrometry (LA-ICP-MS) using a New Wave 213 aperture-imaged, frequency-quintupled laser ablation system (213 nm), coupled to an Agilent 750 quadrupole-based ICP-MS at University College, London. Real time data were processed using GLITTER™. Repeated measurements of external zircon standard Plesovic (reference age determined by thermal ionization mass spectrometry (TIMS) is 337.13 ± 0.37 Ma (Sláma et al., 2008)) and NIST 612 silicate glass (Pearce et al., 1997) were used to correct for instrumental mass bias and depth-dependent inter-element fractionation of Pb, Th and U. Use of time-resolved signals that record the evolving isotopic ratios with depth enabled data filtering to remove spurious signals related to boundaries between inheritance and overgrowths, or inclusions or hidden fractures. Data were filtered using standard discordance tests with a 10% cut-off (Carter and Bristow, 2001). Our provenance conclusions are based on comparison of these ages with published data from bedrock studies, which are usually concordant. However, compilations of Himalayan zircons ages also include slightly discordant data from sediments, in addition to bedrock data, so that comparison between sample data and published results is appropriate. In order to test this issue further we conducted our own study of the bedrock in the Sutlej Valley, treating the grains and data in the same way as the sediments, so that they could be directly compared.

The LA-ICP-MS method results in a single grain age when in reality grains may have complicated growth histories. Using time-resolved (depth) data processing we can detect both cores and overgrowth ages. In sediments detrital zircon grains contain a mixture of euhedral

and rounded grains. The latter are invariably biased towards inherited cores because abrasion in the erosional environment will tend towards removing overgrowths. For this reason it is unrealistic to adopt a sampling strategy focused on dating rims and cores in all grains.

The $^{206}Pb/^{238}U$ ratio was used to determine ages less than 1000 Ma and the $^{207}Pb/^{206}Pb$ ratio for grains older than 1000 Ma. We switch from using the $^{206}Pb/^{238}U$ age to the $^{207}Pb/^{206}Pb$ age for grains older than 1000 Ma because the latter has smaller uncertainties above 1000 Ma. The cross-over point is not fixed and different workers prefer a range between 600 and 1200 Ma. Data were processed using *Isoplot™* (Ludwig, 2003). Uncertainties are typically in the range 1 to 3% and are shown for each analysis in Table 1 for the river sediments and Table 2 for the Sutlej Valley bedrocks. More than 100 grains were analyzed from each sample in order to provide a statistically robust image of what is potentially a complex source terrain, following the recommendations of Ruhl and Hodges (2005).

In addition to U–Pb dating sand samples from each tributary were analyzed for a suite of major and trace elements. This was done primarily to determine Zr concentrations, which are considered to be a good proxy for the zircon content of the sediment (Amidon et al., 2005b). This allows a correction to be made for the differing concentrations when modelling the zircon sediment budget of the river. Samples were powdered in an agate mill before being analyzed for major element oxides (except NaO) using a SPECTRO XEPOS Benchtop Energy Dispersive X-ray Fluorescence (ED-XRF) at University of Massachusetts, Boston (Smith, 2007). Powdered samples (3–5 g dry weight) were measured under He purge. We used U.S. Geological Survey (USGS) Standard Devonian Shale (SDO-1) as the calibration standard and USGS Standard Green River Shale (SGR-1) was analyzed as an unknown to monitor accuracy for this and the major element analyses. Measured values for SGR-1 were better than 95% of the known values. Reported errors represent the propagated error of repeat/replicate measures and the MC ratio for each element, with uncertainties of <5%.

Acid digested samples were quantified for Na concentrations using a PerkinElmer Optima 3000XL Inductively Coupled Plasma Spectrometer (ICP-OES) at University of Massachusetts, Boston. Samples were measured in triplicate under Ar purge using a nebulizer gas flow; we measured the samples using a three point calibration curve (500, 20 and 10 ppm Na). The three-point calibration served as verification for instrument accuracy and precision.

Zirconium concentrations, along with other trace and rare earth elements, were analyzed by Dynamic Reaction Cell Inductively Coupled Plasma Mass Spectrometry (PerkinElmer DRCII ICP-MS) at the University of Massachusetts, Boston. Sixteen milligrams of powdered samples was dissolved completely through ultra-pure acid digestion (Murray and Leinen, 1993). Samples were digested using 7 mL Savillex teflon digestion jars and a hot plate (200–260 °C) for silicate digestion (Algeo et al., 2007), organic removal (Bayon et al., 2002), and removal of residual HF. Samples were digested for 24 h and dried down repetitively after each digestion step. Once the samples were dried down after the removal of concentrated HF, they were acidified with 0.5 mL of concentrated ultrapure HNO_3 and diluted with 50 mL of milli-q water. An internal standard containing 20 ppb of Indium was added to each blank, standard, and sample; the internal standard was used to correct for instrument drift (Abanda and Hannigan, 2006). Major and trace element results are shown in Table 3.

5. Results

5.1. Bulk sediment chemistry

The major element composition of fluvial sediments is largely controlled by the grainsize, as well as the composition of the source rocks. We here consider the composition of the Indus sands using the strength of chemical weathering as measured by the Chemical Index of Alteration (CIA). This is a proxy developed by Nesbitt and Young (1982) that is based on the relative mobility of Na, K and Ca in

Table 1
Analytical results from U–Pb dating of detrital zircon grains by laser ablation ICP-MS.

								Apparent ages (Ma)						Corr.% discordant			
Grain	Pb (ppm)	U (ppm)	Atomic Th/U	206Pb/238U	±1 sigma	207Pb/235U	±1 sigma	206Pb/238U	±2 sigma	207Pb/235U	±2 sigma	207Pb/206Pb	±2 sigma	206/238 207/235	207/206 206/238	Best age (Ma)	±2 sigma
Indus River at Attock																	
L1	5	1770	0.2	0.0028	0.00003	0.01880	0.00048	18.3	4.0	18.9	4.6	69.9	6.7	3.3	73.9	18.3	4.0
Chak-310, dune sand																	
L1	5	1641	0.6	0.0027	0.00003	0.01776	0.00034	17.4	1.5	17.9	1.9	76.4	4.0	2.4	77.2	17.4	1.5
Jhelum River																	
L1	24.5	4575.6	1.53	0.0039	0.00005	0.02767	0.00089	25.3	3.0	27.7	3.6	238.1	10.3	8.5	89.4	25.3	3.0
Chenab River																	
L1	7.1	609.8	1.16	0.0095	0.00019	0.06306	0.00578	61.1	4.4	62.1	8.8	158.8	17.2	1.6	61.5	61.1	4.4
Ravi River																	
L1	106	3168	0.01	0.0367	0.00050	0.28188	0.00522	232.0	8.8	252.1	10.7	426.0	11.2	8.0	45.5	232.0	8.8
Beas River at Mandi																	
L1	8.3	149.6	0.81	0.0491	0.0004	0.3859	0.0033	308.7	17.4	331.4	18.5	471.3	17.8	6.8	34.5	308.7	17.4
Sutlej River																	
L1	6	722	0.8	0.0074	0.00017	0.04709	0.00256	47.3	4.1	46.7	7.6	139.2	16.0	−1.2	66.0	47.3	4.1
Ghaggar River																	
L1	4	326	0.60	0.0105	0.00028	0.06843	0.00488	67.2	10.5	67.2	17.7	273.9	41.2	0.0	75.5	67.2	10.5
River Yamuna																	
L1	338	7421	0.10	0.0483	0.00061	0.33900	0.00414	304.0	10.7	296.4	12.1	603.2	11.1	−2.6	49.6	296.4	12.1

For a complete data set of this table, see Supplementary data.

Table 2
Analytical results from U–Pb dating of zircon grains from basement rocks within the Sutlej Valley, as documented by Vannay et al. (2004) laser ablation ICP-MS.

Grain	Pb (ppm)	U (ppm)	Atomic Th/U	206Pb/238U	±1 sigma	207Pb/235U	±1 sigma	Apparent ages (Ma) 206Pb/238U	±2 sigma	207Pb/235U	±2 sigma	207Pb/206Pb	±2 sigma	Corr.% discordant 206/238 207/235	207/206 206/238	Best age (Ma)	±2 sigma
Sample 32/97 — Greater Himalayan Crystalline Series																	
G1	156	942	0.4	0.16074	0.00147	0.0011	0.9140	1000.3	10.8	960.9	17.7	955.2	16.1	−0.6	−0.7	1000.3	10.8
G2	85	548	0.5	0.1462	0.00144	0.0012	0.9228	1010.3	16.8	879.6	17.5	871.1	20.2	−1.0	−0.2	1010.3	16.8
G3	147	1043	0.5	0.13329	0.00123	0.0045	1.5934	1083.2	12.1	806.6	15.3	871.7	15.8	7.5	3.6	1083.2	12.1
G4	122	269	0.8	0.38692	0.00384	0.0067	0.9251	2198.5	18.7	2108.5	37.0	2087.8	26.1	−1.0	−5.1	2087.8	26.1
G5	1	177	0.4	0.71989	0.00666	0.0014	0.9178	3439.7	14.3	3495.6	51.2	3350.3	23.7	−4.3	−2.1	878.8	15.9
G6	107	662	0.7	0.14818	0.00136	0.0042	0.9184	911.8	11.0	890.8	16.6	878.8	15.9	−1.4	−3.0	911.8	11.0
G7	167	325	0.5	0.4595	0.00422	0.0013	0.9435	2540.6	14.0	2437.3	38.6	2452.4	22.5	0.6	−1.1	2452.4	22.5
G8	39	295	0.2	0.13461	0.00127	0.0015	0.9125	1085.6	14.4	814.1	15.8	853.2	17.4	4.6	−1.9	1085.6	14.4
G9	164	1040	0.2	0.1611	0.00147	0.0015	0.9238	980.3	10.4	962.9	17.6	972.5	15.9	1.0	−0.9	980.3	10.4
G10	113	686	0.3	0.16346	0.00151	0.0015	0.9503	1178.9	12.4	976.0	18.1	1027.9	17.2	5.0	3.9	1027.9	17.2
G11	42	277	0.2	0.1568	0.00149	0.0013	0.9244	913.3	13.5	939.0	17.9	888.3	18.2	−5.7	−6.3	913.3	13.5
G12	88	634	0.3	0.13739	0.00127	0.0015	0.9650	884.6	11.1	829.9	15.7	839.1	15.6	1.1	−1.7	884.6	11.1
G13	35	216	0.4	0.15648	0.00151	0.0017	0.9948	921.6	14.9	937.2	18.2	902.1	19.3	−3.9	−6.7	921.6	14.9
G14	144	717	0.9	0.17062	0.00157	0.0015	0.9578	1084.2	11.5	1015.5	18.6	1008.3	16.9	−0.7	−11.1	1084.2	11.5
G15	37	218	0.7	0.15347	0.00147	0.0013	0.9129	889.4	14.3	920.4	17.8	869.4	18.8	−5.9	−8.6	889.4	14.3
G16	248	1636	0.4	0.14569	0.00133	0.0015	0.9516	951.9	10.0	876.8	16.3	903.2	15.1	2.9	−1.8	951.9	10.0
G17	43	268	0.4	0.15447	0.00147	0.0041	0.9142	851.7	13.3	926.0	17.7	852.6	18.2	−8.6	−8.7	851.7	13.3
G18	372	720	0.7	0.44412	0.00406	0.0013	0.9690	2524.4	13.7	2369.1	37.6	2417.2	22.2	2.0	−3.6	2417.2	22.2
G19	48	318	0.6	0.13829	0.00134	0.0015	0.9738	1055.3	15.8	835.0	16.5	827.2	18.8	−0.9	−14.5	1055.3	15.8
G20	38	236	0.4	0.15301	0.00149	0.0010	0.9150	954.8	15.3	917.8	18.0	866.3	19.5	−5.9	−7.4	954.8	15.3
G21	242	1495	0.3	0.15828	0.00146	0.0022	0.9156	1051.5	11.7	947.2	17.6	964.6	16.6	1.8	−2.2	1051.5	11.7
G22	340	1435	0.1	0.24356	0.00223	0.0015	0.9472	1534.2	12.4	1405.2	24.4	1452.2	19.2	3.2	2.0	1452.2	19.2
G23	98	603	0.3	0.15942	0.00151	0.0012	0.9321	731.7	11.5	953.6	18.1	895.1	17.4	−6.5	−12.4	731.7	11.5
G24	127	985	0.2	0.13196	0.00123	0.0014	0.9501	798.1	10.6	799.0	15.3	811.8	15.2	1.6	−4.6	798.1	10.6
G25	61	392	0.4	0.14841	0.00141	0.0015	0.9367	922.2	13.1	892.0	17.2	857.8	17.6	−4.0	−9.1	922.2	13.1
G26	86	552	0.2	0.15586	0.00146	0.0014	0.9350	970.6	12.2	933.7	17.6	917.5	17.0	−1.8	−3.4	970.6	12.2
G27	107	676	0.5	0.14759	0.00138	0.0013	0.9896	895.1	11.5	887.4	16.8	878.0	16.4	−1.1	−3.6	895.1	11.5
G28	52	353	0.6	0.13238	0.00131	0.0044	0.9170	1091.1	17.2	801.4	16.2	843.7	19.5	5.0	−9.4	1091.1	17.2
G29	499	942	0.4	0.4831	0.00443	0.0013	0.9238	2765.6	14.0	2540.8	39.8	2664.4	22.7	4.6	2.5	2664.4	22.7
G30	140	975	0.5	0.13747	0.00127	0.0016	0.9924	878.0	10.6	830.3	15.7	842.4	15.3	1.4	−2.2	878.0	10.6
G31	35	200	0.6	0.16022	0.00159	0.0031	0.9848	929.8	16.5	958.0	19.0	872.6	20.9	−9.8	−7.6	929.8	16.5
G32	46	134	0.4	0.31377	0.00309	0.0031	0.9359	1629.3	17.8	1759.2	31.6	1585.3	24.7	−11.0	−7.8	1585.3	24.7
G33	173	525	0.2	0.32695	0.00306	0.0038	0.9160	1849.0	14.6	1823.6	31.1	1806.0	22.0	−1.0	−0.7	1806.0	22.0
G34	796	1808	0.3	0.41703	0.00382	0.0013	0.9287	2475.4	13.9	2247.0	36.1	2379.8	22.2	5.6	3.0	2379.8	22.2
Sample 56/96 — Lesser Himalayan Crystalline Series																	
G35	150	957	0.6	0.14429	0.00134	0.0066	1.0042	881.0	11.0	868.9	16.4	865.10	15.80	−0.4	−4.5	881.0	11.0
G36	283	978	0.1	0.29618	0.00274	0.0029	0.9265	1815.5	13.7	1672.3	28.6	1721.7	20.9	2.9	2.8	1721.7	20.9
G37	254	795	0.2	0.31731	0.00294	0.0029	0.9272	1882.2	14.0	1776.6	30.1	1823.6	21.4	2.6	1.3	1823.6	21.4
G38	270	871	0.2	0.30954	0.00287	0.0028	0.9233	1947.9	14.1	1738.4	29.6	1842.6	21.4	5.7	4.1	1842.6	21.4
G39	402	1305	0.2	0.30544	0.00282	0.0038	0.9255	1826.9	13.6	1718.2	29.2	1766.1	21.0	2.7	1.4	1766.1	21.0
G40	371	802	0.6	0.40844	0.00378	0.0030	0.9281	2296.4	14.4	2207.8	35.9	2271.8	22.6	2.8	−1.5	2271.8	22.6
G41	284	853	0.2	0.32646	0.00303	0.0031	0.9285	1845.5	13.8	1821.2	30.8	1827.9	21.4	0.4	−0.9	1827.9	21.4
G42	260	763	0.2	0.33278	0.00309	0.0030	0.9270	1851.3	14.1	1851.8	31.2	1845.9	21.7	−0.3	−1.5	1845.9	21.7
G43	379	1173	0.2	0.31931	0.00296	0.0029	0.9308	1861.9	13.9	1786.4	30.2	1822.2	21.4	2.0	0.6	1822.2	21.4
G44	271	880	0.2	0.30727	0.00286	0.0031	0.9303	1842.6	14.2	1727.3	29.5	1768.9	21.4	2.4	1.7	1768.9	21.4
G45	291	882	0.1	0.32892	0.00306	0.0022	0.9351	1866.0	14.2	1833.1	31.0	1846.0	21.7	0.7	−0.2	1846.0	21.7
G46	250	553	0.2	0.43688	0.00422	0.0024	0.9321	2632.3	17.3	2336.7	39.2	2518.5	25.2	7.2	7.3	2518.5	25.2
G47	335	1311	0.2	0.25535	0.00238	0.0032	0.9364	1803.5	14.3	1466.0	25.8	1617.9	20.9	9.4	6.8	1617.9	20.9
G48	198	571	0.2	0.33854	0.00317	0.0022	0.9296	1859.7	14.8	1879.6	31.9	1869.5	22.3	−0.5	−2.0	1869.5	22.3
G49	191	559	0.2	0.33364	0.00313	0.0034	0.9397	1895.9	15.1	1856.0	31.6	1839.3	22.4	−0.9	−0.6	1839.3	22.4
G50	264	704	0.2	0.36395	0.00342	0.0032	0.9354	2270.6	15.6	2000.9	33.7	2118.6	23.2	5.6	6.6	2118.6	23.2
G51	247	722	0.2	0.33783	0.00316	0.0031	0.9365	1891.1	15.0	1876.2	31.8	1854.2	22.4	−1.2	−0.8	1854.2	22.4
G52	271	795	0.2	0.33529	0.00314	0.0024	0.9329	1853.3	14.9	1864.0	31.6	1841.3	22.3	−1.2	−1.6	1841.3	22.3
G53	359	1419	0.1	0.25834	0.00241	0.0032	0.9457	1778.2	14.6	1481.3	26.0	1610.3	21.1	8.0	6.8	1610.3	21.1
G54	204	596	0.2	0.33627	0.00318	0.0032	0.9351	1857.1	15.4	1868.7	32.0	1848.1	22.8	−1.1	−1.7	1848.1	22.8
G55	402	1129	0.3	0.34006	0.00318	0.0029	0.9411	2177.0	15.4	1887.0	31.9	2021.6	22.8	6.7	5.4	2021.6	22.8
G56	327	986	0.4	0.31239	0.00294	0.0030	0.9465	1889.9	15.4	1752.5	30.2	1806.5	22.5	3.0	0.7	1806.5	22.5
G57	174	545	0.1	0.31801	0.00301	0.0029	0.9385	1828.1	15.6	1780.0	30.8	1800.2	22.7	1.1	−0.1	1800.2	22.7
G58	382	1235	0.2	0.31007	0.00291	0.0017	0.9404	1815.9	14.9	1741.1	30.0	1761.8	22.0	1.2	0.9	1761.8	22.0
G59	288	833	0.2	0.34048	0.00320	0.0031	0.9542	1849.3	15.3	1889.0	32.1	1864.7	22.7	−1.3	−2.2	1864.7	22.7
G60	131	385	0.3	0.32804	0.00313	0.0029	0.9473	1846.9	16.2	1828.9	31.7	1783.3	23.3	−2.6	−1.6	1783.3	23.3
G61	331	1108	0.1	0.30824	0.00292	0.0031	0.9454	2029.1	16.1	1732.0	30.1	1862.6	23.0	7.0	7.0	1862.6	23.0
G62	310	932	0.1	0.33106	0.00313	0.0029	0.9491	1867.3	15.5	1843.5	31.6	1863.7	22.8	1.1	−0.4	1763.5	22.8
G63	203	645	0.2	0.30872	0.00293	0.0028	0.9442	1829.9	15.9	1734.4	30.2	1763.5	22.8	1.6	0.7	1763.5	22.8
G64	326	1113	0.2	0.2923	0.00276	0.0025	0.9454	1834.2	15.4	1653.0	28.9	1734.3	22.2	4.7	3.4	1633.6	22.0
G65	253	968	0.1	0.26654	0.00252	0.0033	0.9639	1786.6	15.6	1523.2	27.0	1633.6	22.0	6.8	5.5	1844.7	24.2
G66	101	270	0.5	0.34444	0.00332	0.0032	0.9473	1883.2	17.1	1908.0	33.2	1844.7	24.2	−3.4	−3.8	1844.7	24.2
G67	312	903	0.2	0.33465	0.00317	0.0030	0.9453	1855.7	15.9	1860.9	31.9	1849.0	23.1	−0.6	−1.8	1849.0	23.1
G68	466	1380	0.4	0.31417	0.00297	0.0030	0.9511	1875.5	15.8	1761.2	30.5	1807.7	22.8	2.6	−0.2	1807.7	22.8

Table 2 (*continued*)

Grain	Pb (ppm)	U (ppm)	Atomic Th/U	206Pb/238U	±1 sigma	207Pb/235U	±1 sigma	Apparent ages (Ma) 206Pb/238U	±2 sigma	207Pb/235U	±2 sigma	207Pb/206Pb	±2 sigma	Corr.% discordant 206/238 207/235	207/206 206/238	Best age (Ma)	±2 sigma
Sample 56/96 — Lesser Himalayan Crystalline Series																	
G69	359	1126	0.1	0.31962	0.00304	0.0033	0.9613	1890.8	16.1	1787.9	31.0	1844.6	23.1	3.1	1.6	1844.6	23.1
G70	159	454	0.2	0.33809	0.00325	0.0032	0.9576	1862.7	16.9	1877.5	32.6	1856.8	24.0	−1.1	−2.0	1856.8	24.0
G71	185	483	0.7	0.33624	0.00322	0.0029	0.9542	1868.6	16.7	1868.6	32.4	1851.4	23.8	−0.9	−5.6	1851.4	23.8
G72	286	916	0.3	0.30498	0.00291	0.0031	0.9568	1835.4	16.5	1716.0	30.1	1748.6	23.2	1.9	1.3	1748.6	23.2
G73	250	733	0.3	0.32712	0.00313	0.0030	0.9526	1857.5	16.6	1824.4	31.7	1815.5	23.6	−0.5	−1.1	1815.5	23.6
G74	347	1081	0.2	0.31807	0.00303	0.0031	0.9537	1818.1	16.4	1780.3	31.0	1796.4	23.3	0.9	−0.3	1796.4	23.3
G75	343	1032	0.2	0.32715	0.00312	0.0037	1.0231	1856.8	16.5	1824.6	31.6	1841.3	23.5	0.9	−0.5	1841.3	23.5
G76	75	200	0.2	0.36166	0.00370	0.0033	0.9755	1882.4	20.8	1990.0	36.4	1809.9	27.8	−10.0	−4.3	1809.9	27.8
G77	172	511	0.1	0.33419	0.00326	0.0032	0.9606	1851.9	18.0	1858.7	32.8	1845.5	24.9	−0.7	−1.3	1845.5	24.9
G78	218	647	0.2	0.3321	0.00319	0.0032	0.9541	1842.6	17.0	1848.6	32.2	1798.8	24.0	−2.8	−1.5	1798.8	24.0
G79	401	1160	0.3	0.33436	0.00319	0.0032	0.9585	1848.9	16.7	1859.5	32.1	1854.6	23.7	−0.3	−1.9	1854.6	23.7
G80	289	857	0.2	0.33489	0.00321	0.0033	0.9621	1849.2	16.8	1862.0	32.3	1851.1	23.9	−0.6	−1.4	1851.1	23.9
G81	253	709	0.2	0.34613	0.00333	0.0032	0.9608	1863.8	17.2	1916.1	33.2	1872.1	24.3	−2.3	−2.8	1872.1	24.3
G82	297	871	0.3	0.32992	0.00317	0.0033	0.9682	1853.5	17.1	1838.0	32.1	1836.4	24.0	−0.1	−1.3	1836.4	24.0
G83	185	525	0.3	0.3398	0.00329	0.0032	0.9656	1856.8	17.7	1885.7	33.0	1845.8	24.6	−2.2	−2.5	1845.8	24.6
G84	185	554	0.2	0.32726	0.00316	0.0020	0.9616	1924.5	17.9	1825.1	32.0	1866.9	24.6	2.2	1.0	1866.9	24.6
G85	213	611	0.3	0.33493	0.00324	0.0056	#DIV/0!	1848.5	17.6	1862.2	32.6	1831.6	24.5	−1.7	−2.1	1831.6	24.5
Sample HB61/96 — Lesser Himalayan Crystalline Series																	
G86	841	3488	0.7	0.22853	0.00207	3.2989	0.0368	1716.8	13.9	1326.8	24.4	1480.8	20.3	10.4	4.0	1480.8	20.3
G87	319	1064	0.1	0.30363	0.00279	4.6739	0.07277	1794.4	15.1	1709.3	30.3	1762.6	22.3	3.0	1.4	1762.6	22.3
G88	513	1926	0.0	0.27779	0.00256	4.2080	0.06455	1797.9	15.3	1580.2	28.5	1675.6	22.1	5.7	5.2	1675.6	22.1
G89	325	1028	0.2	0.31525	0.00285	4.9140	0.05165	1858.4	13.8	1766.5	30.6	1804.7	21.5	2.1	1.2	1804.7	21.5
G90	560	1686	0.0	0.3432	0.00310	6.8197	0.06676	2272.9	14.2	1902.0	32.4	2088.3	22.2	8.9	8.7	2088.3	22.2
G91	477	1724	0.1	0.286	0.00259	4.3958	0.04374	1822.1	13.6	1621.5	28.7	1711.6	21.1	5.3	5.0	1711.6	21.1
G92	308	1008	0.1	0.3104	0.00284	4.8402	0.05688	1857.9	14.4	1742.7	30.6	1791.9	22.0	2.7	2.1	1791.9	22.0
G93	429	1521	0.1	0.28681	0.00266	4.3501	0.05942	1818.8	15.3	1625.6	29.3	1702.9	22.4	4.5	4.0	1702.9	22.4
G94	433	1543	0.1	0.2837	0.00260	4.1586	0.04491	1771.9	14.4	1610.0	28.8	1665.9	21.7	3.4	2.9	1665.9	21.7
G95	387	1272	0.1	0.30901	0.00284	4.7484	0.0518	1842.4	14.6	1735.8	30.7	1775.8	22.1	2.3	1.9	1775.8	22.1
Sample HB27/97 — Tethyan Himalayan																	
G96	39	509	0.1	0.08069	0.00081	0.6175	0.01268	563.0	15.3	500.2	12.4	488.3	16.9	−2.4	−5.5	563.0	15.3
G97	74	827	0.1	0.09488	0.00098	0.7954	0.01867	732.3	18.7	584.3	14.2	594.2	19.8	1.7	−1.4	732.3	18.7
G98	101	607	0.1	0.17146	0.00167	1.7524	0.03392	1175.1	17.7	1020.2	21.1	1028.1	21.9	0.8	0.7	1028.1	21.9
G99	55	731	0.1	0.08017	0.00077	0.5866	0.00938	440.0	11.2	497.1	11.9	468.7	14.5	−6.1	−7.4	440.0	11.2
G100	1053	15271	0.0	0.07476	0.00069	0.6030	0.00495	512.7	8.4	464.8	11.0	479.1	11.5	3.0	3.7	512.7	8.4
G101	68	906	0.0	0.08082	0.00077	0.6347	0.00945	518.8	11.6	501.0	11.9	499.0	14.2	−0.4	−5.7	518.8	11.6
G102	110	1472	0.2	0.07562	0.00071	0.5975	0.00777	516.1	10.7	469.9	11.2	475.6	13.1	1.2	−5.3	516.1	10.7
G103	105	1428	0.0	0.07864	0.00074	0.5997	0.0077	478.3	10.1	488.0	11.5	477.1	13.1	−2.3	−3.1	478.3	10.1
G104	51	508	0.0	0.10914	0.00107	0.8577	0.01536	671.0	14.4	667.8	15.1	628.9	17.8	−6.2	−1.2	671.0	14.4
G105	43	529	0.3	0.0813	0.00087	0.6780	0.01738	727.4	20.8	503.9	13.1	525.6	20.0	4.1	−3.3	727.4	20.8
G106	99	1222	0.3	0.08142	0.00077	0.6253	0.00839	484.6	10.4	504.6	11.9	493.2	13.6	−2.3	−4.2	484.6	10.4
G107	39	495	0.2	0.08123	0.00081	0.6129	0.01209	509.2	14.0	503.5	12.3	485.4	16.4	−3.7	−8.1	509.2	14.0
G108	37	436	0.1	0.08717	0.00094	0.6579	0.0176	558.2	18.5	538.8	13.8	513.3	20.6	−5.0	−23.2	558.2	18.5
G109	52	548	0.3	0.09552	0.00094	0.7609	0.0133	636.1	14.2	588.1	13.8	574.5	16.8	−2.4	−7.8	636.1	14.2
G110	35	430	0.2	0.08236	0.00083	0.6299	0.01281	541.4	14.8	510.2	12.6	496.0	16.9	−2.9	−8.5	541.4	14.8
G111	109	1472	0.1	0.0782	0.00075	0.6086	0.00876	495.4	11.1	485.4	11.7	482.7	13.8	−0.6	−2.5	495.4	11.1
G112	121	1470	0.1	0.08735	0.00085	0.8028	0.01268	786.9	14.8	539.8	12.8	598.4	15.8	9.8	3.9	786.9	14.8
G113	57	392	0.3	0.13824	0.00176	1.2859	0.05748	944.4	32.5	834.7	22.6	839.5	34.6	0.6	−18.6	944.4	32.5
G114	68	908	0.2	0.07678	0.00075	0.6124	0.01006	556.4	12.9	476.9	11.7	485.1	14.7	1.7	−1.8	556.4	12.9
G115	213	2857	0.1	0.07996	0.00075	0.6469	0.0076	563.0	10.6	495.9	11.6	506.5	13.2	2.1	2.4	563.0	10.6
G116	46	604	0.1	0.08083	0.00080	0.6280	0.0109	518.0	12.8	501.1	12.2	494.8	15.3	−1.3	−5.4	518.0	12.8
G117	95	1249	0.2	0.07747	0.00074	0.6527	0.0092	594.5	12.0	481.0	11.5	510.2	13.8	5.7	−1.8	594.5	12.0
G118	81	964	0.5	0.07901	0.00075	0.6109	0.00825	468.5	10.3	490.2	11.7	484.1	13.4	−1.3	−6.5	468.5	10.3
G119	44	486	0.2	0.09188	0.00093	0.7207	0.01455	574.8	14.8	566.6	13.7	551.1	17.6	−2.8	−9.1	574.8	14.8
G120	100	988	0.2	0.10279	0.00098	0.8797	0.01226	714.3	12.9	630.7	14.1	640.8	15.9	1.6	−6.4	714.3	12.9
G121	87	985	0.3	0.08801	0.00084	0.7252	0.01004	630.4	12.3	543.8	12.6	553.8	14.7	1.8	−6.9	630.4	12.3
G122	82	1025	0.1	0.08365	0.00083	0.7187	0.01303	718.3	15.7	517.9	12.6	549.9	16.5	5.8	−3.2	718.3	15.7
G123	48	495	0.1	0.10112	0.00100	0.8383	0.01491	720.7	15.2	621.0	14.4	618.2	17.6	−0.5	−2.1	720.7	15.2
G124	34	384	0.5	0.08384	0.00087	0.6490	0.01436	538.4	15.6	519.0	13.0	507.8	17.9	−2.2	−4.4	538.4	15.6
G125	93	1279	0.1	0.07795	0.00075	0.6181	0.00833	487.7	10.6	483.9	11.7	488.6	13.5	1.0	−2.5	487.7	10.6
G126	62	770	0.3	0.07936	0.00078	0.6609	0.01138	630.4	14.3	492.3	12.0	515.1	15.5	4.4	−0.9	630.4	14.3
G127	183	2511	0.2	0.07542	0.00072	0.6147	0.008	523.3	10.8	468.7	11.3	486.5	13.2	3.7	6.6	523.3	10.8
G128	112	925	0.2	0.1222	0.00119	1.1190	0.01813	828.4	14.9	743.2	16.4	762.5	18.3	2.5	−3.2	828.4	14.9
G129	83	1058	0.3	0.07971	0.00077	0.6249	0.00919	504.3	11.4	494.4	11.9	492.9	14.2	−0.3	−2.2	504.3	11.4
G130	78	766	0.1	0.10492	0.00104	1.0105	0.01778	945.0	17.2	643.2	14.8	709.1	18.5	9.3	0.1	945.0	17.2
G131	70	852	0.2	0.08493	0.00083	0.7285	0.0114	708.6	14.2	525.5	12.6	555.7	15.6	5.4	0.0	708.6	14.2
Samples HB63/96 and HB43/96 — Lesser Himalayan Crystalline Series																	
G132	226	662	0.22	0.33387	0.00305	5.1488	0.05913	1865.6	13.3	1857.1	31.5	1844.2	21.2	−0.7	−1.3	1844.2	21.2
G133	311	1149	0.23	0.2693	0.00246	4.0193	0.04389	1789.8	13.3	1537.2	27.0	1638.1	20.5	6.2	4.9	1638.1	20.5

(*continued on next page*)

Table 2 (*continued*)

Grain	Pb (ppm)	U (ppm)	Atomic Th/U	206Pb/238U	±1 sigma	207Pb/235U	±1 sigma	Apparent ages (Ma) 206Pb/238U	±2 sigma	207Pb/235U	±2 sigma	207Pb/206Pb	±2 sigma	Corr.% discordant 206/238 / 207/235	207/206 / 206/238	Best age (Ma)	±2 sigma
Samples HB63/96 and HB43/96 — Lesser Himalayan Crystalline Series																	
G134	291	1122	0.50	0.24501	0.00224	3.5991	0.04	1774.6	13.5	1412.7	25.2	1549.3	20.2	8.8	6.0	1549.3	20.2
G135	257	743	0.30	0.33236	0.00303	5.1376	0.0511	1863.8	13.0	1849.8	31.4	1842.3	21.0	−0.4	−1.7	1842.3	21.0
G136	89	159	0.45	0.48763	0.00456	9.8882	0.17783	2440.9	15.1	2560.4	41.6	2424.4	23.8	−5.6	−4.4	2424.4	23.8
G137	200	560	0.39	0.33624	0.00310	5.2103	0.0695	1885.5	13.9	1868.6	32.0	1854.3	21.8	−0.8	−2.4	1854.3	21.8
G138	197	521	0.57	0.34057	0.00315	5.1360	0.0754	1853.8	14.2	1889.4	32.3	1842.1	22.0	−2.6	−5.5	1842.1	22.0
G139	107	272	0.51	0.3546	0.00329	5.0891	0.07639	1857.9	14.4	1956.5	33.4	1834.3	22.3	−6.7	−6.5	1834.3	22.3
G140	168	472	0.28	0.34073	0.00315	5.0975	0.0715	1841.3	14.1	1890.2	32.3	1835.7	22.0	−3.0	−3.2	1835.7	22.0
G141	327	1203	0.36	0.26322	0.00241	3.9342	0.04118	1800.2	13.2	1506.3	26.6	1620.7	20.4	7.1	5.2	1620.7	20.4
G142	458	1421	0.38	0.30685	0.00279	4.6823	0.04014	1823.4	12.7	1725.2	29.6	1764.1	20.6	2.2	−0.2	1764.1	20.6
G143	197	539	0.21	0.35374	0.00324	5.5456	0.06278	1917.3	13.4	1952.4	32.9	1907.7	21.5	−2.3	−2.4	1907.7	21.5
G144	194	543	0.27	0.34362	0.00317	5.3921	0.07208	1929.3	14.0	1904.1	32.5	1883.6	21.9	−1.1	−1.3	1883.6	21.9
G145	292	822	0.33	0.33714	0.00308	5.2753	0.0532	1870.6	13.1	1872.9	31.7	1864.9	21.2	−0.4	−2.4	1864.9	21.2
G146	275	915	0.14	0.30291	0.00277	4.5652	0.04488	1831.5	13.1	1705.7	29.5	1742.9	20.8	2.1	2.2	1742.9	20.8
G147	159	420	0.45	0.34819	0.00320	5.2311	0.06545	1857.9	13.8	1925.9	32.7	1857.7	21.7	−3.7	−5.2	1857.7	21.7
G148	251	746	0.27	0.32596	0.00298	5.1712	0.0546	1889.4	13.3	1818.8	31.0	1847.9	21.2	1.6	−0.1	1847.9	21.2
G149	283	802	0.29	0.33875	0.00310	5.1072	0.05289	1830.8	13.1	1880.7	31.9	1837.3	21.2	−2.4	−3.3	1837.3	21.2
G150	248	697	0.41	0.33401	0.00307	5.0663	0.05956	1849.2	13.6	1857.8	31.7	1830.5	21.5	−1.5	−3.2	1830.5	21.5
G151	235	712	0.18	0.32769	0.00300	5.1403	0.05527	1864.8	13.4	1827.2	31.2	1842.8	21.3	0.8	−0.2	1842.8	21.3
G152	274	816	0.17	0.33279	0.00305	5.2482	0.05501	1872.3	13.4	1851.9	31.6	1860.5	21.4	0.5	−0.7	1860.5	21.4
G153	103	276	0.34	0.35081	0.00327	5.1075	0.07815	1837.1	14.6	1938.5	33.3	1837.4	22.4	−5.5	−5.2	1837.4	22.4
G154	126	335	0.39	0.35011	0.00325	5.0661	0.07246	1857.5	14.4	1935.1	33.1	1830.4	22.2	−5.7	−4.9	1830.4	22.2
G155	351	1081	0.21	0.32062	0.00293	4.9478	0.0485	1838.1	13.2	1792.8	30.7	1810.4	21.1	1.0	−0.2	1810.4	21.1
G156	225	633	0.51	0.32612	0.00300	4.8674	0.05595	1831.0	13.7	1819.5	31.2	1796.6	21.5	−1.3	−3.7	1796.6	21.5
G157	129	348	0.34	0.34942	0.00328	5.2758	0.08948	1870.3	15.2	1931.8	33.4	1865.0	22.9	−3.6	−4.1	1865.0	22.9
G158	146	387	0.37	0.35218	0.00331	5.3939	0.09169	1865.2	15.2	1945.0	33.6	1883.9	23.0	−3.2	−4.9	1883.9	23.0
G159	245	613	0.29	0.37937	0.00354	6.7511	0.10432	2144.8	15.0	2073.3	35.1	2079.3	23.1	0.3	0.1	2079.3	23.1
G160	291	845	0.27	0.33321	0.00306	5.1546	0.05512	1848.9	13.5	1853.9	31.6	1845.1	21.4	−0.5	−2.0	1845.1	21.4
G161	246	688	0.52	0.32727	0.00302	5.0035	0.05922	1839.5	13.8	1825.1	31.4	1819.9	21.6	−0.3	−3.8	1819.9	21.6
G162	217	627	0.35	0.32917	0.00304	5.0383	0.06077	1835.4	13.9	1834.4	31.5	1825.8	21.7	−0.5	−2.5	1825.8	21.7
G163	237	654	0.37	0.34201	0.00315	5.2530	0.06048	1871.7	13.8	1896.3	32.3	1861.3	21.8	−1.9	−3.2	1861.3	21.8
G164	126	352	0.42	0.33277	0.00317	5.0238	0.09904	1826.0	16.3	1851.8	32.7	1823.3	23.7	−1.6	−3.9	1823.3	23.7
G165	319	923	0.28	0.33366	0.00308	5.0475	0.05944	1830.0	13.9	1856.1	31.8	1827.3	21.7	−1.6	−2.5	1827.3	21.7
G166	85	214	0.37	0.36688	0.00348	5.0373	0.08908	1853.2	15.7	2014.7	34.9	1825.6	23.5	−10.4	−6.9	1825.6	23.5
G167	246	688	0.64	0.3206	0.00297	4.8841	0.06156	1830.3	14.2	1792.7	31.0	1799.5	21.8	0.4	−4.7	1799.5	21.8
G168	230	432	0.68	0.45458	0.00422	9.3627	0.12834	2388.5	15.0	2415.6	39.5	2374.2	23.5	−1.7	−6.3	2374.2	23.5
G169	255	742	0.27	0.33304	0.00307	5.2112	0.05924	1865.1	14.0	1853.1	31.7	1854.5	21.8	0.1	−1.6	1854.5	21.8
G170	279	526	1.01	0.43207	0.00400	8.8506	0.11481	2409.3	14.9	2315.0	38.1	2322.7	23.3	0.3	−9.0	2322.7	23.3
G171	219	680	0.35	0.30812	0.00287	4.8012	0.06524	1850.1	14.7	1731.4	30.3	1785.1	22.1	3.0	0.5	1785.1	22.1
G172	268	768	0.30	0.33516	0.00310	5.2711	0.06073	1850.6	14.1	1863.3	32.0	1864.2	21.9	0.0	−2.4	1864.2	21.9
G173	904	2663	0.33	0.32656	0.00300	5.1957	0.04599	1862.9	13.6	1821.7	31.2	1851.9	21.4	1.6	−1.2	1851.9	21.4
G174	806	2684	0.38	0.28985	0.00266	4.4657	0.03966	1826.9	13.6	1640.8	28.6	1724.6	21.0	4.9	2.3	1724.6	21.0
G175	704	2141	0.23	0.32321	0.00297	5.1319	0.04799	1855.7	13.8	1805.4	31.0	1841.4	21.5	2.0	−0.2	1841.4	21.5
G176	999	3108	0.28	0.31347	0.00288	4.9459	0.04409	1840.2	13.7	1757.8	30.3	1810.1	21.3	2.9	0.3	1810.1	21.3
G177	1104	3068	0.78	0.31425	0.00289	5.1497	0.04508	1882.5	13.8	1761.6	30.4	1844.3	21.5	4.5	−4.9	1844.3	21.5
G178	781	2172	0.46	0.33438	0.00309	5.1988	0.0548	1848.5	14.1	1859.6	31.9	1852.4	21.9	−0.4	−3.7	1852.4	21.9
G179	439	1359	0.10	0.32686	0.00305	5.0543	0.06777	1874.1	15.0	1823.1	31.7	1828.5	22.5	0.3	0.6	1828.5	22.5
G180	361	1080	0.21	0.32881	0.00305	5.1780	0.06251	1823.2	14.5	1832.6	31.6	1849.0	22.1	0.9	−1.6	1849.0	22.1
G181	585	1704	0.42	0.32303	0.00298	5.0595	0.05073	1847.9	14.1	1804.5	31.1	1829.3	21.7	1.4	−2.0	1829.3	21.7
G182	953	2967	0.37	0.30842	0.00286	4.9191	0.05477	1845.2	14.4	1732.9	30.2	1805.5	21.8	4.0	0.4	1805.5	21.8
G183	874	2815	0.28	0.30441	0.00281	4.8174	0.0483	1836.0	14.3	1713.1	29.8	1787.9	21.7	4.2	1.5	1787.9	21.7
G184	639	2017	0.35	0.30636	0.00283	4.7886	0.04793	1839.5	14.3	1722.8	30.0	1782.9	21.7	3.4	0.7	1782.9	21.7
G185	275	793	0.33	0.33162	0.00309	5.2098	0.06499	1851.3	14.8	1846.2	32.0	1854.2	22.4	0.4	−2.1	1854.2	22.4
G186	530	1656	0.40	0.3044	0.00283	4.7295	0.05577	1839.9	14.7	1713.1	30.0	1772.5	22.0	3.4	0.4	1772.5	22.0
G187	989	3114	0.31	0.30768	0.00286	4.7887	0.05349	1838.7	14.7	1729.3	30.2	1782.9	22.1	3.0	0.7	1782.9	22.1
G188	699	2222	0.41	0.30043	0.00279	4.9050	0.05284	1891.6	14.8	1693.4	29.7	1803.1	22.0	6.1	2.1	1803.1	22.0
G189	779	2414	0.36	0.30927	0.00289	4.9329	0.06274	1844.4	15.2	1737.1	30.5	1807.9	22.4	3.9	0.3	1807.9	22.4
G190	883	2710	0.26	0.3194	0.00296	5.1102	0.05034	1862.1	14.5	1786.8	31.0	1837.8	22.0	2.8	0.3	1837.8	22.0
G191	785	2269	0.32	0.33273	0.00310	5.3277	0.06382	1873.0	15.2	1851.6	32.0	1873.3	22.7	1.2	−1.6	1873.3	22.7
G192	936	2880	0.24	0.31944	0.00297	5.0235	0.05198	1825.8	14.6	1787.0	31.1	1823.3	22.1	2.0	−0.4	1823.3	22.1
G193	468	1286	0.73	0.32189	0.00302	5.0962	0.07092	1849.2	15.7	1799.0	31.5	1835.5	23.0	2.0	−6.2	1835.5	23.0
G194	244	711	0.23	0.3359	0.00315	5.3095	0.07321	1870.0	15.6	1866.9	32.4	1870.4	23.1	0.2	−1.4	1870.4	23.1
G195	607	1773	0.32	0.32913	0.00306	5.1603	0.05598	1837.8	14.9	1834.2	31.7	1846.1	22.4	0.6	−2.0	1846.1	22.4
G196	645	1835	0.58	0.32132	0.00301	5.0596	0.06353	1859.1	15.5	1796.2	31.4	1829.4	22.8	1.8	−3.4	1829.4	22.8
G197	737	2409	0.52	0.29261	0.00272	4.6478	0.0476	1836.8	15.1	1654.6	29.2	1757.9	22.1	5.9	−0.2	1757.9	22.1
G198	747	2183	0.19	0.33808	0.00317	5.4369	0.06637	1839.2	15.6	1877.4	32.6	1890.7	23.1	0.7	−2.0	1890.7	23.1
G199	756	2276	0.36	0.31755	0.00297	5.0174	0.05484	1846.6	15.5	1777.8	31.1	1822.3	22.7	2.4	−0.7	1822.3	22.7
G200	642	1911	0.18	0.33244	0.00311	5.3164	0.05927	1853.5	15.6	1850.2	32.1	1871.5	22.9	1.1	−1.0	1871.5	22.9
G201	1094	4027	0.21	0.27384	0.00256	4.3781	0.04535	1828.6	15.5	1560.3	28.0	1708.2	22.2	8.7	6.0	1708.2	22.2
G202	671	1997	0.21	0.3314	0.00310	5.2911	0.05897	1840.2	15.6	1845.2	32.1	1867.4	23.0	1.2	−1.3	1867.4	23.0
G203	833	2282	0.53	0.33603	0.00317	5.4857	0.0725	1839.5	16.1	1867.5	32.6	1898.4	23.4	1.6	−5.1	1898.4	23.4
G204	642	1907	0.29	0.3263	0.00307	5.1945	0.063	1842.6	15.9	1820.4	31.9	1851.7	23.2	1.7	−1.2	1851.7	23.2
G205	725	2107	0.40	0.32677	0.00306	5.1785	0.05736	1850.1	15.9	1822.7	31.8	1849.1	23.1	1.4	−2.0	1849.1	23.1

Table 2 (*continued*)

Grain	Pb (ppm)	U (ppm)	Atomic Th/U	206Pb/238U	±1 sigma	207Pb/235U	±1 sigma	Apparent ages (Ma) 206Pb/238U	±2 sigma	207Pb/235U	±2 sigma	207Pb/206Pb	±2 sigma	Corr.% discordant 206/238 207/235	207/206 206/238	Best age (Ma)	±2 sigma
Samples HB63/96 and HB43/96 — Lesser Himalayan Crystalline Series																	
G206	579	2196	0.13	0.27051	0.00254	4.1688	0.04663	1803.7	15.8	1543.4	27.8	1667.9	22.4	7.5	6.2	1667.9	22.4
G207	1062	4175	0.13	0.26143	0.00245	4.1514	0.04411	1805.2	15.8	1497.2	27.1	1664.5	22.2	10.1	7.4	1664.5	22.2
G208	740	2353	0.31	0.30627	0.00299	4.7350	0.09732	1898.9	18.9	1722.3	31.6	1773.5	25.4	2.9	2.6	1773.5	25.4
G209	966	3175	0.26	0.29971	0.00281	4.8334	0.05502	1848.9	16.1	1689.9	29.9	1790.7	22.9	5.6	2.6	1790.7	22.9
Sample HB66/96 — MCT myolinite																	
G210	445	1227	0.6	0.3257	0.00306	4.7035	0.08145	1817.5	39.1	1767.9	30.7	1839.1	23.5	−2.8	1.2	1839.1	23.5
G211	403	1140	0.3	0.34072	0.00318	5.0688	0.08296	1890.1	39.9	1830.9	30.5	1887.2	23.1	−3.2	−0.2	1887.2	23.1
G212	402	1222	0.3	0.31694	0.00290	4.9432	0.05669	1774.8	37.7	1809.7	29.1	1844.7	21.7	1.9	3.8	1844.7	21.7
G213	434	1239	0.4	0.32938	0.00302	5.0650	0.05783	1835.4	38.6	1830.3	29.2	1845.7	21.7	−0.3	0.6	1845.7	21.7
G214	314	674	0.3	0.42179	0.00410	8.1601	0.20825	2268.6	46.5	2248.9	33.5	2312.1	25.8	−0.9	1.9	2312.1	25.8
G215	293	890	0.1	0.33533	0.00311	5.2260	0.07685	1864.2	39.4	1856.9	29.9	1866.5	22.5	−0.4	0.1	1866.5	22.5
G216	242	660	0.3	0.3513	0.00325	5.3870	0.07959	1940.8	40.3	1882.8	30.1	1856.0	22.6	−3.1	−4.6	1856.0	22.6
G217	503	1534	0.2	0.32608	0.00299	5.0933	0.0615	1819.4	38.4	1835.0	29.3	1872.7	21.9	0.9	2.8	1872.7	21.9
G218	500	1422	0.7	0.31496	0.00288	5.0692	0.05874	1765.1	37.6	1831.0	29.0	1855.4	21.7	3.6	4.9	1855.4	21.7
G219	421	1217	0.4	0.32989	0.00304	5.1177	0.06625	1837.8	38.8	1839.0	29.5	1847.1	22.0	0.1	0.5	1847.1	22.0
G220	353	1100	0.1	0.32866	0.00302	5.3154	0.06845	1831.9	38.6	1871.3	29.5	1911.4	22.1	2.1	4.2	1911.4	22.1
G221	280	803	0.3	0.33513	0.00313	5.1702	0.0859	1863.2	39.6	1847.7	30.4	1869.8	23.1	−0.8	0.4	1869.8	23.1
G222	294	870	0.2	0.33396	0.00308	5.3831	0.07314	1857.5	39.1	1882.2	29.7	1909.4	22.3	1.3	2.7	1909.4	22.3
G223	278	801	0.2	0.34375	0.00317	5.2653	0.07304	1904.7	39.8	1863.2	29.8	1855.6	22.3	−2.2	−2.6	1855.6	22.3
G224	196	601	0.4	0.30707	0.00286	4.5317	0.06908	1726.3	37.6	1736.8	29.9	1848.2	22.9	0.6	6.6	1848.2	22.9
G225	278	807	0.3	0.33473	0.00308	5.0978	0.06593	1861.3	39.1	1835.7	29.6	1864.0	22.1	−1.4	0.1	1864.0	22.1
G226	516	1532	0.2	0.32934	0.00301	5.2365	0.0557	1835.2	38.5	1858.6	29.0	1848.9	21.4	1.3	0.7	1848.9	21.4
G227	486	1429	0.3	0.33064	0.00302	5.1959	0.0577	1841.5	38.6	1851.9	29.1	1839.4	21.6	0.6	−0.1	1839.4	21.6
G228	400	1157	0.5	0.32261	0.00296	5.0714	0.06137	1802.5	38.2	1831.3	29.3	1880.7	21.8	1.6	4.2	1880.7	21.8
G229	247	692	0.5	0.33072	0.00307	5.0884	0.07749	1841.9	39.1	1834.2	30.2	1903.7	22.9	−0.4	3.2	1903.7	22.9
G230	314	901	0.3	0.3317	0.00312	5.2677	0.09468	1846.6	39.5	1863.6	30.8	1879.7	23.6	0.9	1.8	1879.7	23.6
G231	107	239	0.9	0.37544	0.00358	5.3190	0.10976	2054.9	42.9	1871.9	31.9	1877.7	24.4	−9.8	−9.4	1877.7	24.4
G232	427	919	0.4	0.42823	0.00394	9.0825	0.12513	2297.7	44.9	2346.3	30.8	2368.2	22.7	2.1	3.0	2368.2	22.7
Sample HB31/97 — Lesser Himalayan Crystalline Series																	
G233	142	424	0.4	0.31651	0.00291	5.0340	0.06553	1772.7	28.9	1825.1	19.6	1904.0	11.7	2.9	6.9	1904.0	11.7
G234	302	889	0.4	0.3184	0.00289	4.9964	0.04515	1781.9	28.6	1818.7	18.8	1853.0	10.6	2.0	3.8	1853.0	10.6
G235	153	466	0.3	0.31478	0.00289	4.8831	0.05782	1764.2	28.7	1799.3	19.4	1870.1	11.4	2.0	5.7	1870.1	11.4
G236	133	387	0.3	0.3273	0.00306	5.0290	0.08423	1825.3	30.1	1824.2	20.6	1866.2	13.0	−0.1	2.2	1866.2	13.0
G237	312	898	0.4	0.32852	0.00299	5.1667	0.05041	1831.2	29.4	1847.1	19.1	1874.4	10.8	0.9	2.3	1874.4	10.8
G238	371	1135	0.3	0.31281	0.00284	5.0210	0.04511	1754.5	28.3	1822.9	18.7	1868.4	10.6	3.7	6.1	1868.4	10.6
G239	118	331	0.4	0.33576	0.00310	5.0262	0.06862	1866.2	30.3	1823.7	19.9	1864.3	11.9	−2.3	−0.1	1864.3	11.9
G240	159	468	0.3	0.32569	0.00299	4.8864	0.06042	1817.5	29.5	1799.9	19.5	1862.1	11.5	−1.0	2.4	1862.1	11.5
G241	134	389	0.3	0.32711	0.00301	4.9114	0.06276	1824.4	29.6	1804.2	19.6	1860.5	11.6	−1.1	1.9	1860.5	11.6
G242	213	624	0.4	0.31961	0.00292	4.9823	0.05416	1787.8	28.9	1816.3	19.2	1875.0	11.1	1.6	4.7	1875.0	11.1
G243	263	863	0.3	0.29092	0.00268	4.3767	0.05713	1646.1	27.2	1707.9	19.3	1794.8	11.7	3.6	8.3	1794.8	11.7
G244	300	817	0.6	0.32957	0.00303	5.1937	0.06701	1836.3	29.8	1851.6	19.6	1850.9	11.5	0.8	0.8	1850.9	11.5
G245	102	286	0.3	0.33768	0.00314	4.9670	0.0744	1875.5	30.7	1813.7	20.3	1874.1	12.3	−3.4	−0.1	1874.1	12.3
G246	200	559	0.5	0.33097	0.00303	5.1617	0.05992	1843.1	29.7	1846.3	19.4	1873.4	11.3	0.2	1.6	1873.4	11.3
G247	273	763	0.6	0.32128	0.00293	5.0268	0.05222	1796.0	29.0	1823.8	19.0	1854.8	10.9	1.5	3.2	1854.8	10.9
G248	268	867	0.3	0.29759	0.00274	4.6252	0.0602	1679.3	27.6	1753.8	19.4	1843.9	11.9	4.2	8.9	1843.9	11.9
G249	241	744	0.1	0.32448	0.00300	5.1598	0.07477	1811.6	29.6	1846.0	20.0	1884.9	12.1	1.9	3.9	1884.9	12.1
G250	141	377	0.5	0.33989	0.00314	5.0283	0.07107	1886.1	30.6	1824.1	20.0	1875.5	12.0	−3.4	−0.6	1875.5	12.0
G251	485	1551	0.2	0.31302	0.00286	4.8786	0.0506	1755.6	28.5	1798.6	19.1	1861.3	11.0	2.4	5.7	1861.3	11.0
G252	155	460	0.3	0.32326	0.00297	4.9849	0.06342	1805.6	29.3	1816.8	19.6	1861.0	11.6	0.6	3.0	1861.0	11.6
G253	145	404	0.4	0.3359	0.00309	4.9828	0.06493	1866.9	30.2	1816.4	19.7	1850.1	11.7	−2.8	−0.9	1850.1	11.7
G254	566	1741	0.4	0.30675	0.00278	4.8784	0.03829	1724.7	27.8	1798.5	18.5	1838.9	10.4	4.1	6.2	1838.9	10.4
G255	488	1564	0.3	0.29871	0.00271	4.7248	0.04052	1684.9	27.3	1771.6	18.5	1844.5	10.5	4.9	8.7	1844.5	10.5
G256	199	609	0.2	0.32142	0.00294	4.7811	0.05344	1796.7	29.1	1781.6	19.3	1847.4	11.2	−0.8	2.7	1847.4	11.2
G257	166	442	0.4	0.3482	0.00321	5.1535	0.07131	1926.0	31.1	1845.0	20.0	1840.2	11.9	−4.4	−4.7	1840.2	11.9
G258	277	786	0.4	0.32751	0.00299	5.0258	0.05208	1826.3	29.4	1823.7	19.1	1860.5	10.9	−0.1	1.8	1860.5	10.9
G259	130	350	0.5	0.341	0.00316	4.9921	0.07196	1891.5	30.8	1818.0	20.1	1848.9	12.1	−4.0	−2.3	1848.9	12.1
G260	165	498	0.3	0.31534	0.00293	4.7330	0.06959	1766.9	29.1	1773.1	20.0	1841.2	12.3	0.3	4.0	1841.2	12.3
G261	393	1255	0.3	0.30364	0.00279	4.5832	0.05725	1709.3	28.0	1746.2	19.3	1823.2	11.6	2.1	6.2	1823.2	11.6
G262	397	1203	0.4	0.30962	0.00283	4.9303	0.0515	1738.8	28.2	1807.4	19.0	1864.9	11.0	3.8	6.8	1864.9	11.0
G263	207	589	0.4	0.32853	0.00301	5.0174	0.05769	1831.3	29.6	1822.3	19.4	1872.2	11.3	−0.5	2.2	1872.2	11.3
G264	87	220	0.4	0.36528	0.00342	4.9507	0.08213	2007.2	32.7	1810.9	20.9	1839.5	12.8	−10.8	−9.1	1839.5	12.8
G265	522	1681	0.3	0.29853	0.00271	4.6880	0.04012	1684.0	27.3	1765.1	18.5	1830.8	10.5	4.6	8.0	1830.8	10.5
G266	303	882	0.4	0.31983	0.00292	4.9791	0.05344	1788.9	28.9	1815.8	19.1	1851.6	11.1	1.5	3.4	1851.6	11.1
G267	125	361	0.3	0.33293	0.00308	4.8045	0.06526	1852.6	30.2	1785.7	19.9	1869.2	11.9	−3.7	0.9	1869.2	11.9
G268	133	371	0.3	0.3382	0.00312	4.9853	0.06829	1878.0	30.4	1816.8	19.9	1856.4	11.9	−3.4	−1.2	1856.4	11.9

Table 3
Major and trace element concentrations of the sediments analyzed from the tributaries of the Indus River, measured by XRF and ICP-MS respectively. Major element concentrations are shown as weight percentages, while trace elements are in ppm. Nd isotope values are from Tripathi et al. (2004) for the Yamuna and Ghaggar and Clift et al. (2002) for the other streams.

Samples	Sc	V	Cr	Co	Ni	Cu	Zn	Rb	Sr	Sr	Y	Zr	Nb	Cs	Ba
Beas	5.75	46.91	33.01	39.38	19.00	13.12	11.69	110.82	64.13	65.42	16.37	14.84	7.35	8.18	707.56
Chenab	4.93	43.62	33.62	82.63	19.34	9.71	12.61	75.77	85.91	86.76	13.81	29.18	7.60	4.18	487.43
Ghaggar	4.43	48.14	41.86	85.10	25.77	13.86	11.62	51.58	31.75	31.89	15.02	49.14	4.14	2.63	408.33
Indus upstream	10.21	75.71	62.93	130.47	25.44	16.86	10.77	76.41	250.09	268.07	21.59	17.87	3.98	2.82	685.86
Jhelum	7.94	71.97	74.89	74.06	41.98	30.43	14.30	88.33	138.52	141.50	19.64	62.72	10.60	5.37	529.91
Ravi	6.49	64.63	40.54	92.06	26.80	12.49	11.32	106.14	54.98	55.78	16.42	38.80	7.54	5.05	792.10
Sutlej	5.25	40.35	31.92	127.12	18.71	12.19	11.25	80.05	71.33	72.40	15.71	14.26	6.35	6.09	413.56
Yamuna	9.18	64.59	41.75	22.83	24.94	19.34	15.30	127.12	78.07	79.89	23.22	55.29	8.03	5.91	656.21

Samples	Ba	La	Ce	Pr	Nd	Sm	Eu	Gd	Tb	Dy	Ho	Er	Tm	Yb	Lu
Beas	428.78	27.02	54.43	5.74	22.31	4.34	0.72	4.03	0.56	3.04	0.59	1.59	0.18	1.47	0.23
Chenab	294.34	25.24	50.75	5.51	21.73	4.12	0.85	3.76	0.50	2.74	0.50	1.36	0.15	1.23	0.18
Ghaggar	245.33	27.68	55.61	6.02	23.64	4.43	0.77	3.95	0.52	2.87	0.53	1.51	0.17	1.36	0.20
Indusupstream	408.61	35.76	67.70	7.02	27.02	4.95	0.97	4.26	0.68	3.49	0.67	2.03	0.32	2.37	0.32
Jhelum	320.11	29.66	60.25	6.52	25.69	4.99	1.00	4.72	0.67	3.72	0.73	2.03	0.23	1.81	0.27
Ravi	471.59	34.09	67.99	7.48	29.41	5.75	1.07	4.70	0.68	3.17	0.55	1.54	0.20	1.47	0.20
Sutlej	249.92	25.75	50.28	5.33	20.12	3.81	0.60	3.46	0.49	2.67	0.54	1.56	0.17	1.30	0.20
Yamuna	390.10	41.41	88.14	10.17	42.53	8.91	1.44	6.91	1.01	4.26	0.75	2.23	0.33	2.52	0.32

Samples	Hf	Ta	Pb	Th	U	Li	Be	Ge	Mo	Sn	εNd
Beas	0.44	0.87	19.77	16.27	8.72	30.16	1.47	1.04	17.79	BDL	unknown
Chenab	0.81	1.51	20.33	11.23	5.33	18.87	1.02	1.00	19.50	BDL	−15
Ghaggar	BDL	0.76	13.25	13.06	5.57	17.71	0.70	0.97	19.53	BDL	−15.6
Indus upstream	BDL	0.92	20.60	16.11	7.05	21.11	1.82	1.30	19.59	2.16	−10.8
Jhelum	0.77	1.93	17.75	16.07	7.30	27.11	1.13	0.93	15.61	BDL	−15.4
Ravi	BDL	1.68	17.10	13.88	6.23	23.33	1.19	1.43	19.84	BDL	−15.1
Sutlej	BDL	1.90	14.01	14.55	8.31	17.81	1.64	0.81	17.46	BDL	−19
Yamuna	1.75	0.76	23.87	22.23	10.72	26.90	1.81	1.73	22.10	10.51	−17.7

Samples	Na_2O	MgO	Al_2O_3	SiO_2	P_2O_5	K_2O	CaO	TiO_2	MnO	Fe_2O_3	Total
Beas	1.46	1.92	10.93	77.63	0.13	2.93	2.03	0.47	0.06	3.16	100.72
Chenab	1.08	2.23	9.46	52.28	0.11	2.13	3.03	0.37	0.06	3.19	73.93
Ghaggar	0.46	0.35	6.83	82.58	0.12	1.44	2.16	0.55	0.07	3.58	98.13
Indus upstream	2.05	2.20	11.11	69.74	0.12	2.11	5.34	0.46	0.09	4.04	97.27
Jhelum	1.03	3.77	10.44	47.12	0.11	2.02	6.07	0.58	0.06	4.60	75.80
Ravi	1.13	1.96	10.28	82.04	0.13	2.49	1.26	0.54	0.06	3.37	103.25
Sutlej	1.03	1.62	7.47	82.54	0.13	2.00	3.38	0.47	0.05	3.25	101.94
Yamuna	1.21	2.82	13.45	68.85	0.12	2.97	2.32	0.55	0.05	3.96	96.31

aqueous fluids, compared to immobile Al, which tends to be concentrated in the residues of weathered rocks. CIA is calculated as follows:

$$CIA = \left(\frac{A1_2O_3}{A1_2O_3 + CaO* + Na_2O + K_2O} \right) \times 100.$$

CIA is derived from the molecular weights of the oxides. The CaO* value used is only the calcium content from the silicate fraction of the sediment and correction must be made for the carbonate and phosphate contents. No attempt was made to dissolve carbonate before analysis. In this study we follow the method of Singh et al. (2005) in using P_2O_5 to correct for phosphate content. Subsequently, a correction is made for carbonate based on assuming a reasonable Ca/Na ratio for silicate continental material. If the remaining number of moles after the phosphate correction is still more than the number of Na_2O moles then this latter value is used as a proxy for CaO* value. Uncertainties in the CIA values are in excess of the 3% uncertainty in the XRF analytical data and can be used only as general proxies for weathering intensity.

Fig. 4 shows the Si/Ti (a ratio independent of the carbonate content) versus CIA because this allows the different parts of the Indus River drainage to be compared with one another. Our data show that there is no close relationship between how sandy (higher Si/Ti) a sediment is and the CIA, although the muddiest sediment (Jhelum) does show high degrees of alteration. The trunk Indus, Beas and Sutlej sediments appear to be relatively sandy and only slightly affected by chemical weathering, indicating that physical erosion processes are dominant in their headwaters.

The rare earth element (REE) characteristics of the sediments are considered by normalizing the concentrations against chondite and average continental crust compositions (Fig. 5). The diagrams show that all samples show a relative depletion in Eu, which is a characteristic of plagioclase crystallization in the source rocks. The samples are all enriched in light compared to heavy REEs, and that LREEs are more enriched than is typical for continental crust (Rudnick and Fountain, 1995). Our analyses show that the Yamuna is anomalous in showing higher overall concentrations of REEs and also that the LREEs are less depleted in that sample than in the other river sediments. i.e., that La/Sm is lower in the Yamuna sediment than in the other rivers. However, within the Indus system there are no major compositional differences between the sediments from the different tributaries, showing that these elements cannot be used as effective provenance proxies. Our work is consistent with studies of our Asian river systems that suggested that grain size and sorting characteristics of the sediment were the primary controls on REE compositions (Clift et al., 2008b).

5.2. Zircon ages

The results of our U–Pb dating analyses are displayed graphically in Fig. 6 in the form of probability density functions (PDF), showing

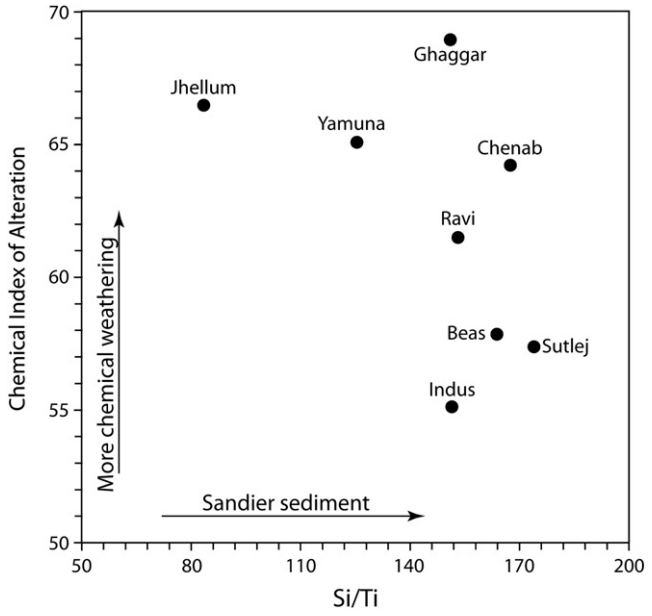

Fig. 4. Discrimination plot showing Chemical Index of Alteration (CIA) plotted against Si/Ti for all samples considered in this study.

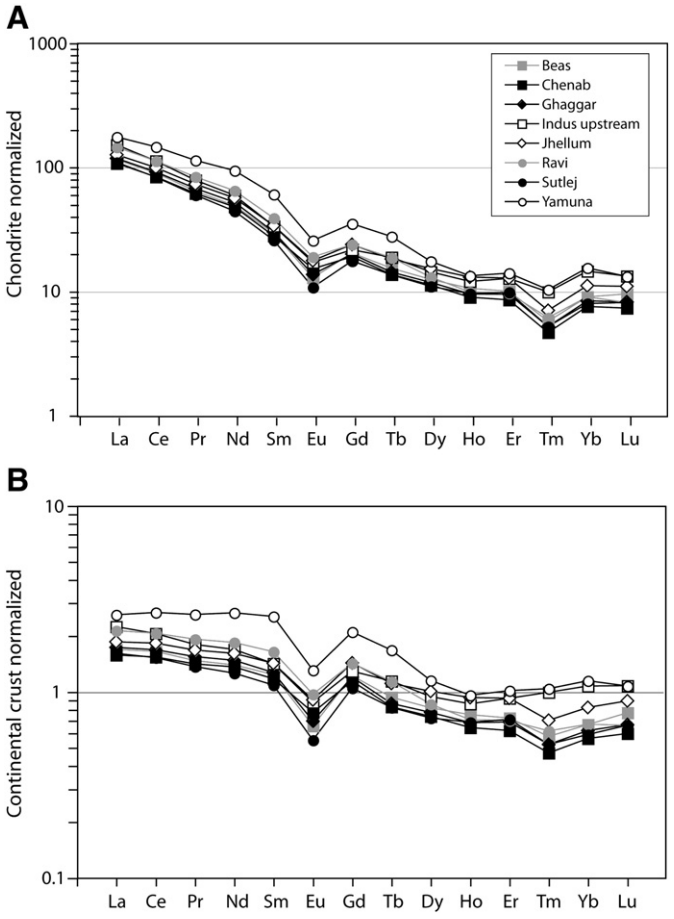

Fig. 5. (A) Chondrite-normalized and (B) continental crust-normalized rare earth element figure for sediment taken from the modern Red River. Sediments are divided in groups: those from the southern Song Da system, those from the northern Song Lo and Song Chay system, those from smaller tributaries and those from the main trunk river. Chondrite values used are from Anders and Grevesse (1989). Continental crust from Rudnick and Fountain (1995). Data is shown in Table 3.

the relative likelihood of encountering a grain of any given age. Although there are a number of common features in the age spectra of different sands, most notably peaks at 400–500, 800–1100 and 1800–1900 Ma, we are able to resolve important differences in the relative strength of these peaks. The Indus River above Attock Bridge (Fig. 1) is particularly distinctive in showing a dominance of grains younger than 200 Ma (Fig. 6A). Only the Jhelum also shows a major younger population, although even here this group has declined to only ~11% of the total, compared with 59% at Attock Bridge. The neighbouring Chenab comprises <4% of grains <200 Ma, east of which grains younger than 200 Ma are very rare, i.e. 1% in the Ravi, 0% in the Beas, 3% in the Sutlej and 1% in the Yamuna. Many of these sands show a prominent, well-defined age peak at ~1800–1900 Ma, as well as a broad population spanning 800 to 1100 Ma.

An important exception to this general pattern is the Beas River, which is characterized by a large 400–500 Ma age population, comprising 32% of the total (Fig. 6E). This age population is also present in significant numbers in the Chenab River (18%), and to a lesser extent to the Jhelum, Ravi, Sutlej and Ghaggar Rivers (5, 5, 6, and 6% respectively). The Yamuna River is dominated by 1800–1900 Ma grains (26% of the total), but also shows significant numbers in the 800–1100 Ma range (33% of the total). In all sands, except the upper Indus, a minority population older than 2 Ga is seen, generally ranging from 5 to 9% of the total. However, the non-unique character of grains older than 2300 Ma means that they are not useful for provenance work and we do not consider them further here.

The U–Pb dates from the bedrock of the Sutlej Valley are shown in Fig. 7B and demonstrate the strong dominance of grains centered around 1850 Ma, very similar to the peak recorded from the Lesser Himalaya (DeCelles et al., 2000). A small number of grains are seen to be dated around 500 Ma (~7.8% lie between 400 and 600 Ma), with another minor population between 800 and 1100 Ma (10.8%). Only 0.4% of the population are dated as being older than 2200 Ma.

6. Discussion

The sources of the sediments into each river can be constrained by comparison with the published bedrock analyses (Fig. 3), as well as with reference to the observed geology of the drainage basins (Fig. 1). We can construct sediment provenance budgets based on zircon age spectra because of the coherent differences between the possible source ranges. We divide up the zircon age populations of each sediment into four groups, which we defined based on the observed ranges of ages in possible sources determined by earlier studies (Fig. 3). Grains dating at 0–300 Ma are associated with erosion from the Karakoram and Transhimalaya, those at 300–750 Ma are linked to erosion of the Tethyan Himalaya, 750–1250 Ma correlate with the Tethyan and Greater Himalaya, and 1500–2300 Ma are eroded dominantly from the Lesser Himalaya. Grains lying outside these groups are not provenance diagnostic and are ignored, although this tends to be a rather small minority in each case. We recognize that there is overlap between the different sources and that a unique provenance designation is impossible for most ages, but we argue that based on the general age character of the basement there are grain ranges that are especially characteristic of certain sources and thus these can be treated as reasonable proxies for the flux from those sources. Using only U–Pb ages it is however impractical to fully separate the Tethyan and Greater Himalaya, especially as dating in the Beas suggests that grains dating at 300–750 Ma may also be found in the Greater Himalaya within the Indus basin (see below).

6.1. Influence of the Siwaliks

Unfortunately, the influence of the Siwaliks cannot be isolated only with U–Pb zircon ages and their erosional influence cannot be accounted for, thus introducing a probable 10–15% error into the

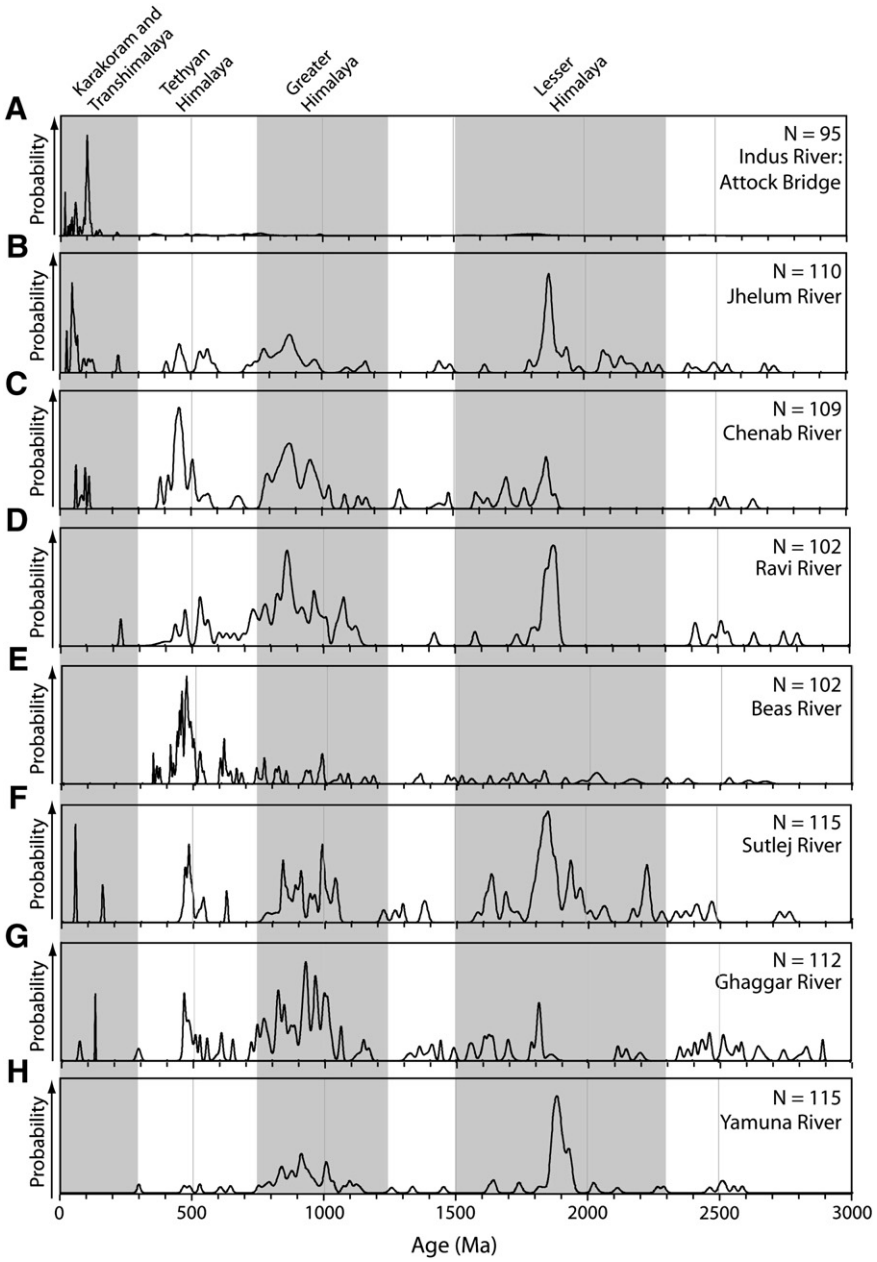

Fig. 6. Probability density plots for zircon age populations in modern rivers of the Indus drainage basin. Data presented in Table 1. See Fig. 1 for locations. Grey bands show typical ranges of possible source rocks.

budget. The only zircon detrital ages from the Siwaliks come from Nepal (DeCelles et al., 1998; Bernet et al., 2006) and may not be applicable to the Indus basin, because of along strike compositional variability and because the river valleys may comprise different proportions of the Lesser, Tethyan and Greater Himalaya, Transhimalaya and Karakoram. In the Nepal case the Siwaliks show a range of zircon ages reflecting their origin as fluvial sediments. Depending on the stability of the source regions the Siwaliks might be expected to have zircon age spectra not so different from the modern river system. Not all the rivers are uniformly influenced by the Siwaliks. Table 4 shows that at one extreme only 7.4% of the Sutlej source regions are underlain by Siwalik rocks, while at the other 45% of the Beas source is Siwalik, albeit downstream of the sample location. The Jhelum, Chenab and Ravi basins comprise 23–26% Siwaliks. Nonetheless, because the Siwaliks are recycling earlier eroded fluvial sediments differences in the zircon populations should reflect real differences in the erosion of the bedrock sources, not just varying input from the Siwaliks, which the Nepal studies indicate to be rather limited.

Table 4 shows that upstream of the sample points the basins contain very different areas of Siwalik outcrop. The Indus and Beas expose no Siwalik Group rocks and in the Sutlej the proportion is <0.8% of the total, suggesting that uncertainties related to erosion of these rocks was correspondingly low. However, the Jhelum, Chenab and Ravi comprise 25.8, 23.1 and 42.0% respectively of Siwaliks upstream of their sample points, which could cause greater uncertainties. The poor match between zircon populations and outcrop areas of bedrock sources in the Jhelum and the Chenab Valleys, discussed below, could reflect strong erosion of the Siwalik outcrop, as well as preferential erosion of the Lesser Himalaya. Interestingly the same does not seem to be true in the Ravi River, which has the greatest proportion of Siwaliks, but which yields a zircon age spectrum quite consistent with the exposed area of

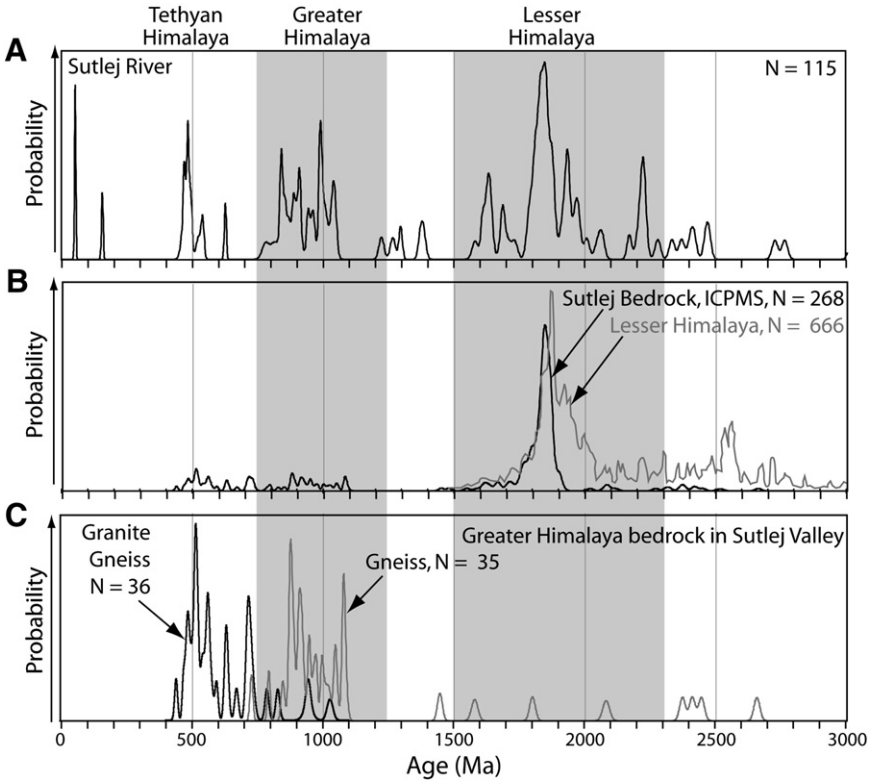

Fig. 7. Probability density plots of U–Pb age from zircons from (A) Sutlej River, (B) bedrock samples from along the course of the Sutlej River and (C) only the Greater Himalayan crystalline bedrocks within the Sutlej Valley. Data in Table 2.

bedrock. This might imply either that Siwalik erosion is not important, or that if it is then the composition of the Siwaliks in the Ravi Valley lies close to what the modern river carries. U–Pb dating alone has no way to resolve between these possibilities.

6.2. Bedrock and fluvial zircons in the Sutlej

Work on Himalayan rivers in Nepal has shown that rock units contribute zircon grains in proportion to their exposed area, i.e. the detrital age populations are representative of the rocks exposed in the drainage basin (Amidon et al., 2005a). We test whether this hypothesis is valid in the Indus basin by comparing our new U–Pb zircon ages from bedrock from the Lesser and Greater Himalaya in the Sutlej Valley with detrital grains in the Sutlej River. Fig. 7 shows that the river sediments and bedrock both share a major peak around 1850 Ma, however the river also has a significant population (23%) of grains dating 750–1250 Ma, which are less apparent in the total bedrock data (Fig. 7B). This represents preferential sampling of certain bedrock units at outcrop because the Greater Himalaya account for 16.2% of the total Sutlej mountain drainage area compared to 8.8% for the Lesser Himalaya. It is noteworthy that basement lithologies with typical Greater Himalaya ages, 750–1250 Ma, as well as younger ones at ~500 Ma are known from exposures (Fig. 7C), but these appear to be more heavily represented in the river sands than in the bedrock data set.

6.3. Zircon budgets and outcrop area

Table 4 and Fig. 8 show percentage estimates of the relative outcrop areas for the major tectonic units within each river source region, including the Sutlej. This shows that in some cases there are major discrepancies between the sources inferred from the zircon budget and the outcrop areas, i.e. that all outcrops do not contribute equally to the river sediment load. This is in contrast to the conclusions of Amidon et al. (2005a) in Nepal. The upper Indus, Ravi and Chenab Rivers do show a generally good match between exposed rock areas and the source inferred by comparing the zircon populations and possible sources. However, the Sutlej and Jhelum Rivers yield much greater volumes of Lesser Himalayan zircons (1500–2300 Ma) than would be expected based on the area of outcrop in these rivers, while the Beas is dominated by Greater Himalaya outcrop. The contrast with the work of Amidon et al. (2005a) may reflect the fact that all the rivers in that study lay within strong monsoonal conditions south of the Himalayan rain shadow, while some of the Indus tributaries show large gradients in climate within the mountainous catchments. Thus, we can show that the bedrock and river zircon ages are comparable, at least in the Sutlej, and that our provenance methods are reliable. However, it is clear that certain parts of each drainage basin may contribute more sediment to the river sediment load than might be expected based on their outcrop area.

6.4. Influence of Nanga Parbat

The young zircon age population in the upper Indus River at Attock Bridge, prior to its mixing with the eastern tributaries, correlates well with the known age range in the Karakoram, Kohistan and the Transhimalaya that dominate the headwaters upstream of this point. Figs. 3A and 9 show the age range for the Karakoram, which accounts for at least 76% of the grains younger than 200 Ma in the Indus at Attock Bridge (i.e., grains dated at 90–120 Ma). In contrast, Kohistan and the Ladakh Batholith, collectively known as the Transhimalaya, represent no more than 22% of the <200 Ma group, based on the number of grains spanning 40–70 Ma, although this age range is non-unique and is also found in the Karakoram. Interestingly, the metamorphic Nanga Parbat Massif does not seem to be a dominant sediment contributor, despite its well documented high exhumation rates (Zeitler, 1985). U–Pb zircon dating of the gneisses of the massif shows grain ages extending back to no more than 15 Ma (Zeitler and Chamberlain, 1991; Zeitler et al., 1993), while only one grain in the Attock Bridge sample comes close to matching that value (Table 1).

Table 4
Compilation showing the percentages that the different zircon groups make to each river's composition, compared to the proportions of the outcrop areas, as shown in Fig. 1. The percentage outcrops are shown in three ways, those areas upstream of the sample location, those areas upstream of the sample location excluding the Siwaliks, and the total basin outcrop north of the Main Frontal Thrust. The percentage of each zircon population group represents the number of grains in each sample that fall within the specified range normalized to 100%, excluding those grains that are not diagnostic and lie outside these groups.

	Indus	Total bedrock			Jhelum	Total bedrock			Chenab	Total bedrock		
	Zircons	Upstream of sample	Without Siwaliks	Total basin	Zircons	Upstream of sample	Without Siwaliks	Total basin	Zircons	Upstream of sample	Without Siwaliks	Total basin
0–300 Ma — Transhimalaya/Karakoram	67.9	69.1	69.1	58.6	13.1	0.0	0.0	0.0	4.1	0.0	0.0	0.0
300–750 Ma — Tethyan Himalaya	10.7	11.6	11.6	7.2	15.2	47.2	63.6	47.2	31.6	17.3	22.4	17.3
750–1250 Ma — Greater Himalaya	7.1	16.4	16.4	11.1	28.3	24.0	32.4	24.0	43.9	52.4	68.1	52.4
1500–2300 Ma — Lesser Himalaya	14.3	2.9	2.9	10.8	43.4	2.9	4.0	2.9	20.4	7.2	9.4	7.2
Siwaliks		0.0	na	12.3		25.8	na	25.8		23.1	na	23.1

This result confirms the conclusions of earlier studies that Nanga Parbat is not a dominant sediment producer in the Indus system (Clift et al., 2002; Garzanti et al., 2005), or at least if it is then its flux is overwhelmed by that from other regions, most notably the Karakoram. Our conclusions are dependent on the assumption that the young age characterization of the massif is truly accurate. It is noteworthy that Nanga Parbat contrasts with the behaviour of the eastern Himalayan syntaxis, where sediment budgets indicate that around 35% of the Brahmaputra sediment load is derived from the Namche Barwe massif (Garzanti et al., 2004).

6.5. Erosion in the Beas Valley

The common presence of a 1800–1900 Ma age peak throughout those rivers draining the Himalaya correlates well with known basement ages in the Lesser Himalaya (Figs. 3D and 7B) and indicates that these ranges are important suppliers of sediment to the Indus Delta. Not surprisingly the 750–1250 Ma grains that characterize the Tethyan and Greater Himalaya are also common constituents of many of the sands. While these age groups are also known from the Siwalik Group we estimate that these strata account for no more than 15% of the total flux (Lavé and Avouac, 2001), and cannot explain grains of this age in the Beas and Sutlej samples, collected upstream of those sources. The Beas River is exceptional in showing a strong peak at 400–500 Ma (37% of total grains), a range associated with the Tethyan Himalaya in Nepal (DeCelles et al., 2004). This river is geographically somewhat smaller than the others considered here and is mapped as draining rocks of the Greater Himalaya, but with almost no Lesser Himalaya in its catchment and just a fragment of the Tethyan Himalaya in its upper reaches (Fig. 1). It is thus possible that the 400–500 Ma grains in the Beas are mostly from the Greater Himalaya (Chail and Jutogh Group), not least because granite gneisses with these ages were found in the Sutlej Valley (Fig. 7C) but were mapped by Vannay et al. (2004) as Greater Himalaya. However, in the Beas Valley there is no major peak around 1000 Ma, which is also typical of the Greater Himalaya. This is enigmatic given the bedrock geology and the topography. We suggest that the Greater Himalaya in the Beas Valley (i.e. the Jutogh and Chail Groups) may differ from those characterized in Nepal (DeCelles et al., 2004) in containing abundant 400–500 Ma grains, but relatively few 1000 Ma grains. The Beas age populations are not explicable from the total age synthesis presented in Fig. 3, but require local bedrock heterogeneity, or a serious misidentification of rock types in the upper Beas catchment.

6.6. Dune sands in the Thar Desert

Our analysis of a dune sand in the NW Thar Desert allows us to place some constraints on the origin of the sediment in this region, although it tells us nothing about when the Thar Desert first began to form, generally believed to be in the Late Pliocene–Pleistocene (Glennie et al., 2002). In Fig. 10 we compare the age spectrum from the dune sand with those from the nearest rivers, the Sutlej and the Ghaggar, as well as the main Indus downstream at Thatta (Fig. 1), which represents the composition of the river after the major tributaries have mixed, but before entering the sea. The dune sand grains show a well-developed age peak at 1800–1900 Ma (Fig. 10C; 18% of total), very similar to that seen in the neighbouring Sutlej sample (Fig. 10B), originally derived from the Lesser Himalaya, and rare in the Ghaggar River. However, the dune sand also contains a significant proportion of grains younger than 200 Ma, which are very rare in the Sutlej and the Ghaggar, but common only in the modern Indus (Fig. 6A and 10A). 20% of the grains in the Thar dunes are younger than 200 Ma, compared to 21% of the grains in the Indus at Thatta, but only 3% in each of the Sutlej and Ghaggar Rivers. This suggests a strong influx of sand from the downstream parts of the Indus into the Thar Desert during the recent geological past, rather than reworking of sediment more locally from the nearest rivers, such as the Sutlej or Ghaggar.

Assuming that our samples are representative of the lower Indus and the Thar Desert the new data require a dominant flux from the Indus into the Thar Desert because a major additional contribution from the Sutlej or Ghaggar would have diluted the <200 Ma grain population to a greater extent than we observe here. The neighbouring Yamuna may have previously flowed west into the Indus, but this is even more depleted in grains <200 Ma and also cannot be a major source of the Thar sands. Drainage capture involving these eastern rivers does not address the enigmatic character of the Thar Desert sands. Deriving the <200 Ma grains more directly from the upper Indus would require a major rerouting of this stream towards the southeast, compared to its present course. While this might in theory be possible there is no evidence of abandoned channels trending in that direction, such as are visible in the Ghaggar region (Ghose et al., 1979; Saini et al., 2009) to indicate that this has happened in the recent geological past. Instead we suggest that the Thar Desert sand was transported SW to NE by eolian processes from the lower Indus around and northeast of Sukkur (Fig. 1), likely during the summer monsoon when this wind direction is dominant and powerful (Xie and Arkin, 1997). Sand dunes geometries on the western side of the Thar Desert indicate a dominant transport towards the NNE (Singhvi et al., 2010) and a variety of climate proxies indicate that the summer monsoon has been strong during interglacial periods throughout the Pleistocene (Clift and Plumb, 2008). Our conclusion is consistent with earlier studies showing that dune accumulation ceased during the LGM, despite arid conditions and only resumed when the summer SW monsoon strengthened again in the Early Holocene (Thomas et al., 1999). If the monsoon wind is essential to dune formation then its effects might be expected also to control provenance.

6.7. Sediment budgets

6.7.1. Zircon-based budgets

We here convert the zircon budgets into sediment volume budgets using the assumption that the various sources have relative equal

Ravi	Total bedrock			Beas	Total bedrock			Sutlej	Total bedrock		
Zircons	Upstream of sample	Without Siwaliks	Total basin	Zircons	Upstream of sample	Without Siwaliks	Total basin	Zircons	Upstream of sample	Without Siwaliks	Total basin
1.1	0.0	0.0	0.0	0.0	0.0	0.0	0.0	3.0	5.0	5.0	4.6
20.7	0.0	0.0	0.0	61.2	4.3	4.3	2.0	10.1	68.0	68.0	63.0
52.2	44.7	60.5	44.7	18.8	95.7	95.7	45.9	27.3	21.0	21.0	19.4
26.1	29.2	39.5	29.2	20.0	0.0	0.0	7.2	59.6	6.0	6.0	5.6
	26.1	na	26.1		0.0	na	44.9		0.0	na	7.4

concentrations of zircons and that certain age grains come from particular sources. Amidon et al. (2005a) showed that different source formations can vary in zircon concentration significantly on km scales. However, when considering the whole Indus basin measuring zircon abundance in all source formations is not practical and none of our samples was taken from a river draining a single tectonic unit that would allow variability to be tested. Nonetheless, our data suggest that large concentration variations do not dominate the zircon budget on the regional scale. While it could be argued that the much greater volume of Lesser Himalayan zircons in the Sutlej, Chenab and the Jhelum Rivers compared to the outcrop area (Fig. 8) could indicate that these source ranges are especially rich in zircons the data from the Ravi and the Beas show the opposite trend. Occum's razor indicates that we should assume approximately similar source zircon concentrations until better source data can improve the budget.

Fig. 11 shows graphically how each sand sample breaks down in terms of the four simplified age groups defined above, corresponding to the major sources. Some large-scale differences are apparent, as they were in the more complex PDF plots (Fig. 3), most notably in the high proportion of grains <300 Ma in the trunk Indus at Attock Bridge, a value that falls significantly downstream as the river is joined by the eastern tributaries, so that older grains dominate by the time the sediment reaches Thatta near the delta. This diagram highlights the fact that, apart from in the upper Indus grains younger than 300 Ma are only commonly found in the Jhelum and to a lesser extent the Chenab. Otherwise they comprise 3% or less of the sediment in the easternmost rivers. The Jhelum drains the southern side of the Nanga Parbat massif and may derive some its young population there. Because the Chenab and eastern rivers do not drain Nanga Parbat, the Karakoram or Transhimalaya the origin of the young grains is unclear. The <300 Ma grains in the Sutlej may derive from the Indus Suture, where this stream rises, but that cannot be the case of the other eastern tributaries. The <300 Ma grains were presumably originally derived from the upper Indus, or at least a palaeo-Jhelum or palaeo-Sutlej. If the upper Indus had previously reached the foreland at a location much further east than its present position then we might expect the foreland sediments in those regions to be rich in young grains, which would then be available for reworking. The fact that none of these rivers does show much evidence for this is consistent with the upper Indus being pinned in the syntaxis and having experienced little drainage evolution of its own, even though there is significant change in the foreland to the east (e.g., Burbank et al., 1996; Clift and Blusztajn, 2005). Fig. 11 further emphasizes the large proportion of grains <300 Ma in the Thar Desert sands, which in turn requires much of the desert sand to be reworked from the lower reaches of the Indus. We note that the general age structure of the zircons in the Thar Desert most closely resembles those in the Indus at Thatta.

The simplified sediment budget shows that the oldest 1500–2300 Ma (Lesser Himalayan) group is the single largest part of the Jhelum, Sutlej and Yamuna River zircon populations, while the 750–1250 Ma (Greater Himalayan) grouping is the largest in the Chenab, Ravi and Ghaggar Rivers. The Beas is anomalous in being dominated by 300–750 Ma grains, reflecting its limited size and high proportion of Greater Himalayan exposure (Table 4, Fig. 8). It is interesting to note that the overall age character of the Siwaliks in Nepal (DeCelles et al., 2004) looks very much like the Yamuna and Sutlej Rivers today, suggesting that the rivers feeding the foreland basin in the Miocene, when these sediments accumulated, must have looked much like these modern rivers do today and that the same type of source rocks had already been exposed at that time. As noted above we do not think that similarities between Yamuna sands and those in the Siwaliks implies that most of the sediment in the Yamuna (or any other stream) is generated by erosion from the Siwaliks.

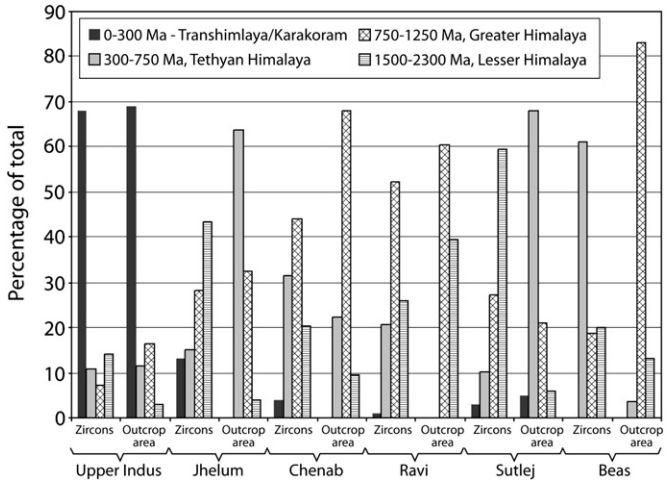

Fig. 8. Histograms comparing the relative proportions of zircon grain ages and the percentage of outcrop areas within each of the upper Indus tributaries. While the upper Indus itself, together with the Ravi and Chenab shows a relatively good correlation, there are major mis-matches in the Jhelum, Beas and Sutlej indicative of high sediment production in specific parts of the drainage.

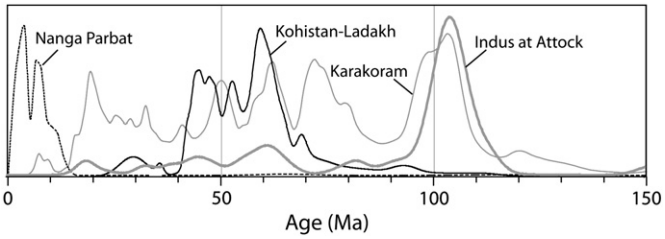

Fig. 9. Probability density plots of U–Pb age from zircons from Attock Bridge compared with possible sources in the Karakoram, Nanga Parbat and Kohistan-Ladakh. The data show that the vast majority of these zircons are eroded in the Karakoram.

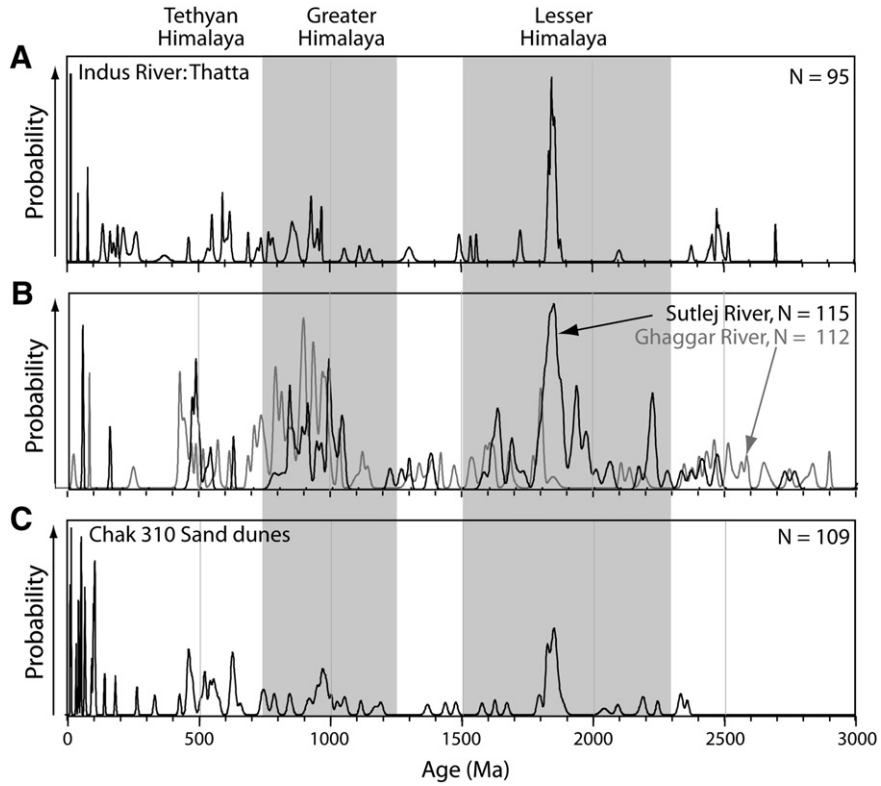

Fig. 10. Probability density plots of U–Pb age from detrital zircon populations sampled at (A) the Indus River at Thatta, near the delta. Data are from Clift et al. (2004) but filtered and replotted using the same criteria as for the new data in this study, (B) the Sutlej River in the Lesser Himalaya, and (C) Thar Desert sands from Marot.

6.8. Origin of the delta sands

Given the age spectra of the major tributaries, we can attempt a simple sediment budget for the lower reaches of the Indus River. The model is presented in Table 5. For each river sample we split the measured zircon population into the four age groups defined above and normalize these to 100% in order to eliminate the non-unique grains. We then simulated the mixing of the river by calculating the bulk composition resulting from combining the five major end-member rivers. We use the Zr concentration data to weight each tributary appropriately given the different zircon concentrations in the sands. In doing this we follow the observation of Amidon (2005b) that zircon concentrations can vary by at least 2–3-fold in rivers draining the Nepal Himalaya. In order to quantify the zircon budget of the Indus flux to the delta we do not need to know the proportion of zircon grains within each sediment, only the relative concentrations of zircon in each. Our objective is to understand how the sediment now sampled at the delta was formed through mixing of the five major modern end member tributaries. To achieve this goal we started with proportions based on the water discharge in each river, but then adjusted the flux from each iteratively until the mis-match between the model sediment and the measured range of zircon ages at Thatta was <3% for all the populations. We endeavour to provide the best possible fit to the observed zircon age spectrum at Thatta, which is shown in Table 6 and graphically in Fig. 12A. This represents our estimate of how much each modern tributary would have to contribute to the Indus in order to make the sand now found at Thatta.

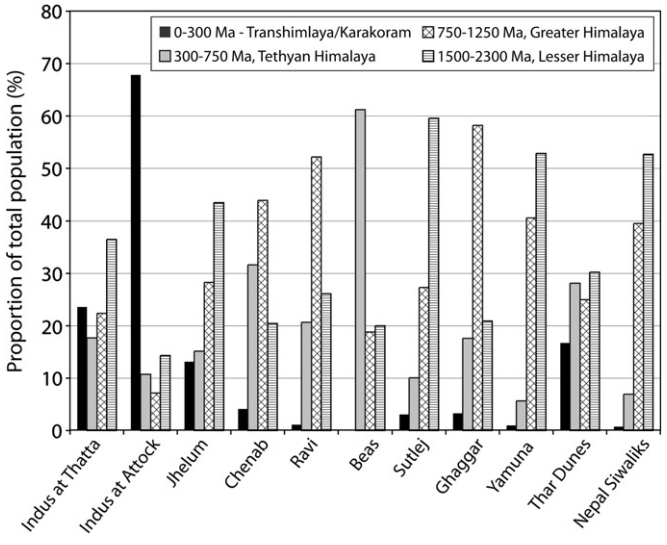

Fig. 11. Simplified break-down of the age populations in the modern Indus sands showing large-scale differences between the major tributaries. Those grains older than 1250 Ma are representative of erosion from the Lesser Himalaya. The proportions are calculated by splitting the grains into the four defined groups, excluding non-unique grains and normalizing to 100%.

Assuming that our samples are representative of the modern outflux from these rivers, it is apparent that much more flux is required from the Sutlej than would be expected from its recent water budget if we are to account for the high proportion of old Lesser Himalayan (1500–2300 Ma) zircons found close to the delta at Thatta. The Jhelum is much richer in zircons than the Sutlej and must be responsible for some of the 1500–2300 Ma grains. However, a budget based on a high Jhelum flux shows worse fit in terms of 0–300 and 300–750 Ma grains. If the Yamuna had previously flowed to the west in the recent geological past and has only recently been captured east into the Ganges then this might account for some of the "excess" 1500–2300 Ma zircons at Thatta. This need for so much flux from the Sutlej reflects the fact that this river, and the Yamuna, stand out in being particularly rich in the 1500–2300 Ma grains compared to other rivers in the system. These grains are relatively abundant at Thatta, despite the fact that modern discharge from the Sutlej is modest.

Table 5
Estimated inputs from different streams studied here to the net flow into the Indus, showing our preferred budget required to match zircon population found at Thatta (Clift et al., 2004). The proportions are normalized to 100% after excluding those grains that do not fall within the provenance-distinctive groups.

	% contribution from each river								Discharge-based model	Modified model	Indus at Thatta
Age groups	Indus	Jhelum	Chenab	Ravi	Beas	Sutlej	Ghaggar	Yamuna	(%)	(%)	
Water discharge (% of total in the modern Indus)	56	14	16	4	4	6	na	na			
0–300 Ma	67.9	13.1	4.1	1.1	0.0	3.0	3.3	0.9	31.0	23.8	23.5
300–750 Ma	10.7	15.2	31.6	20.7	61.2	10.1	17.6	5.7	17.6	16.3	17.6
750–1250 Ma	7.1	28.3	43.9	52.2	18.8	27.3	58.2	40.6	24.1	24.5	22.4
1500–2300 Ma	14.3	43.4	20.4	26.1	20.0	59.6	20.9	52.8	27.3	35.4	36.5
% of total sediment flux in modern Indus at Thatta	34	9	9	2	5	41	na	na			
Epsilon Nd	−10.8	−15.4	−15.0	−15.1	−19.0	−19.0			−12.8	−15.2	−15.0

Conversely, the Chenab River appears to be contributing much less sediment than would be assumed from its water discharge, because the 750–1250 Ma grains that are common in that stream are not so abundant lower in the river system. The same would also be true of the Ravi River, but because this is small its load is not critical to the overall mass balance.

6.8.1. Water-based budgets

An alternative way to predict what the composition of Indus River sands should be is to use the modern water discharge from the rivers (Table 6). In this approach we estimate what the mixed river sediment would look like if the sediments were combined in the same ratio as the water, assuming that greater water flux carries more sediment. Again the sediment budget has to be weighted using the Zr concentrations to account for the contrasting zircon concentrations in each tributary. Average water budgets for the Indus, Jhelum and Chenab were derived from records spanning the annual records from 1922 to 2009, while those from the Sutlej, Beas and Ravi are taken from 1947 to 1955.

We exercise care in assuming that sediment carrying power is linearly linked to water discharge averages because the sediment carrying capacity of rivers is complicated and controlled by more than total annual water discharge (Milliman, 1997). Rivers that are susceptible to flash flooding after dry seasons generally carry more sediment per unit of water than those with a more continuous discharge. Seasonality and storminess of the precipitation are known to affect the erosive regime (Molnar, 2001). However, in a single river system that is neither transport-limited or detachment limited it has been demonstrated that temporal variations in suspended sediment discharge are related to the water discharge (Subramanian, 1996; Robinson et al., 2007). Ali and De Boer (2007) showed that there was a strong link between suspended sediment load and the water discharge in the upper Indus basin. If the geology and the climate are similar in adjacent river systems then those with high water discharge will tend to carry the greater sediment load (Kao and Milliman, 2008). Thus, in the limited area of the western Himalaya, where all the rivers are affected by the summer monsoon rains and drain similar rock types, a broad correlation between water discharge and sediment load would be expected. A potentially complicating factor is that while the link between water discharge and suspended load is well understood in the Indus (Ali and De Boer, 2007, 2008) the same is not true of the bedload, where most of the zircon transport is expected, because of this mineral's high density. Nonetheless, the water discharge may be used as a proxy for the carrying power of the stream and we would anticipate that those streams with a strong discharge would also be transporting the most solid sediment. Clearly this rule is disrupted by modern damming and would have varied in the past as a result of natural damming by landslides, especially in the Early-Mid Miocene (Bookhagen et al., 2005). Our model sediment attempts to model the sediment flux to the ocean prior to dam construction.

Our model budget was compared to the measured age spectrum of sediment from the lower reaches of the river at Thatta, as the two might be expected to be comparable (Fig. 1) (Clift et al., 2004). The model was also cross-checked using bulk sediment Nd isotope data (Clift et al., 2002) to determine whether this is a good model for the sediment budget, although the Nd method is relatively insensitive to modest changes in flux from the different Himalayan tributaries. The Nd model uses the Nd concentrations for each tributary's sediment (Table 3) and assumes that, like the zircon, the sediments are mixed in the proportion of the water discharge to estimate what the homogenized mixed sediment composition would be (Table 5).

Our water discharge-based sediment model does not yield a very good match to the age spectrum at Thatta, specifically under-predicting the number of grains in the 1500–2300 Ma range (27% predicted versus 43% measured) and overpredicted by >50% the number of <300 Ma grains as has been observed. This could imply that the water discharge is largely decoupled from the zircon transportation process or that the sediment now at the delta was not eroded in the present regime.

6.9. Temporal instability

Why the water and zircon-based sediment budgets are so different could be related to fundamental differences between the catchments that we are not accounting for, i.e., that there is not a strong link between total annual discharge and bedload sediment flux. For example, the Sutlej and Yamuna River erode a wide swath of the Lesser Himalaya, while the Ravi, Jhelum and Chenab cross only a modest strip of these rocks, and their drainages are dominated by the Greater Himalaya. If the Lesser Himalaya were composed of friable, easily eroded, zircon-rich rock then this could explain the apparently productive character of the Sutlej in the zircon budget. While the Greater Himalaya are composed of granitoids and gneisses, the Lesser Himalaya contain a significant proportion of more erodable schists and low grade metamorphic rocks, although hard crystalline rocks are also present, especially in the Upper Lesser Himalaya (Valdiya, 1980).

Lithological differences may explain some of the discrepancies in zircon yield, with some rocks being much richer in zircons than others (Amidon et al., 2005a). However, there is no data to support that possibility and here we suggest that varying sediment transport rates could provide an explanation for the mis-match between the modern discharge from the mountains and the composition of the delta sediment. Zircon grains are very dense minerals and are not transported instantaneously to the delta after their initial erosion. In the Indus we propose that zircons take 5000–10,000 yr to reach the delta. This figure is based on the observed lag between clay-dominated bulk sediment Nd compositions and zircon U–Pb dates in the Indus delta (Clift et al., 2010). While Nd isotopes are seen to change with the intensifying monsoon at the onset of the Holocene (14–9 ka), zircons are much slower to respond and only change at the delta between 7 ka and the present (Clift et al., 2010). This implies a lag time of around 5–10 k.y. for the transport of zircons to the river's lower reaches a distance of ~1200 km across the flood plains. Thus, we

Table 6
Water discharge records for the major tributaries of the Indus used to model the expected sediment flux to the modern river. Data for the Sutlej, Ravi, Yamuna and Beas are from the Irrigation and Power Research Institute Punjab, India (unpublished). Data from the Indus, Jhelum and Chenab are from personal communication with the Pakistan Commissioner for Indus Waters.

Indus at Kalabagh			Jhelum at Mangla		Chenab at Marala	
	32° 54′ 59.16″N	71° 31′ 43.10″E	33° 07.776″N	73° 38.311′E	32° 40′ 11.37″N	74° 28′ 07.59″E
Years	Discharge (ac ft/s)	Discharge (m^3/s)	Discharge (ac ft/s)	Discharge (m^3/s)	Discharge (ac ft/s)	Discharge (m^3/s)
1922–23	97.69	4,255,376	25.76	1,122,106	23.99	1,045,004
1923–24	110.04	4,793,342	22.93	998,831	21.04	916,502
1924–25	82.70	3,602,412	26.46	1,152,598	20.53	894,287
1925–26	77.76	3,387,226	20.74	903,434	20.23	881,219
1926–27	72.86	3,173,782	22.39	975,308	22.06	960,934
1927–28	69.73	3,037,439	20.69	901,256	20.41	889,060
1928–29	81.12	3,533,587	27.22	1,185,703	21.97	957,013
1929–30	76.67	3,339,745	23.57	1,026,709	23.90	1,041,084
1930–31	86.41	3,764,020	25.58	1,114,265	24.87	1,083,337
1931–32	78.06	3,400,294	25.30	1,102,068	20.04	872,942
1932–33	82.05	3,574,098	21.34	929,570	21.87	952,657
1933–34	91.85	4,000,986	26.18	1,140,401	26.42	1,150,855
1934–35	86.07	3,749,209	18.02	784,951	22.77	991,861
1935–36	87.43	3,808,451	25.80	1,123,848	25.86	1,126,462
1936–37	95.69	4,168,256	24.31	1,058,944	25.82	1,124,719
1937–38	87.53	3,812,807	21.03	916,067	22.88	996,653
1938–39	95.66	4,166,950	23.60	1,028,016	28.69	1,249,736
1939–40	100.05	4,358,178	22.09	962,240	22.64	986,198
1940–41	84.91	3,698,680	16.54	720,482	18.65	812,394
1941–42	91.29	3,976,592	19.77	861,181	22.61	984,892
1942–43	112.62	4,905,727	25.63	1,116,443	28.83	1,255,835
1943–44	95.36	4,153,882	23.26	1,013,206	28.38	1,236,233
1944–45	92.33	4,021,895	19.43	846,371	24.40	1,062,864
1945–46	105.11	4,578,592	20.67	900,385	24.72	1,076,803
1946–47	90.26	3,931,726	15.35	668,646	23.25	1,012,770
1947–48	78.32	3,411,619	17.82	776,239	28.53	1,242,767
1948–49	95.10	4,142,556	27.80	1,210,968	32.82	1,429,639
1949–50	104.10	4,534,596	24.74	1,077,674	27.16	1,183,090
1950–51	106.34	4,632,170	30.19	1,315,076	35.13	1,530,263
1951–52	71.93	3,133,271	20.57	896,029	21.31	928,264
1952–53	86.45	3,765,762	19.57	852,469	24.28	1,057,637
1953–54	93.57	4,075,909	22.68	987,941	26.83	1,168,715
1954–55	90.81	3,955,684	23.70	1,032,372	25.74	1,121,234
1955–56	84.27	3,670,801	19.32	841,579	28.94	1,260,626
1956–57	98.79	4,303,292	25.02	1,089,871	33.57	1,462,309
1957–58	85.87	3,740,497	32.74	1,426,154	32.49	1,415,264
1958–59	99.47	4,332,913	27.40	1,193,544	31.69	1,380,416
1959–60	120.09	5,231,120	31.65	1,378,674	35.05	1,526,778
1960–61	104.51	4,552,456	16.26	708,286	24.94	1,086,386
1961–62	93.85	4,088,106	17.79	774,932	28.87	1,257,577
1962–63	71.33	3,107,135	16.17	704,365	22.31	971,824
1963–64	89.36	3,892,522	22.01	958,756	23.69	1,031,936
1964–65	88.73	3,865,079	23.60	1,028,016	26.10	1,136,916
1965–66	89.74	3,909,074	26.60	1,158,696	22.64	986,198
1966–67	91.47	3,984,433	23.10	1,006,236	25.90	1,128,204
1967–68	96.98	4,224,449	23.90	1,041,084	25.31	1,102,504
1968–69	93.29	4,063,712	21.64	942,638	23.91	1,041,520
1969–70	87.50	3,811,500	24.21	1,054,588	22.55	982,278
1970–71	71.52	3,115,411	15.35	668,646	19.30	840,708
1971–72	71.74	3,124,994	13.55	590,238	18.85	821,106
1972–73	79.58	3,466,505	24.96	1,087,258	21.53	937,847
1973–74	106.69	4,647,416	26.44	1,151,726	30.96	1,348,618
1974–75	63.19	2,752,556	16.32	710,899	18.23	794,099
1975–76	81.65	3,556,674	25.39	1,105,988	32.84	1,430,510
1976–77	81.54	3,551,882	24.65	1,073,754	29.18	1,271,081
1977–78	81.23	3,538,379	19.63	855,083	26.60	1,158,696
1978–79	106.58	4,642,625	24.62	1,072,447	32.28	1,406,117
1979–80	86.99	3,789,284	20.71	902,128	24.28	1,057,637
1980–81	86.76	3,779,266	23.44	1,021,046	26.19	1,140,836
1981–82	89.94	3,917,786	22.59	984,020	28.09	1,223,600
1982–83	73.24	3,190,334	21.33	929,135	27.80	1,210,968
1983–84	93.91	4,090,720	26.22	1,142,143	29.82	1,298,959
1984–85	92.17	4,014,925	18.67	813,265	24.08	1,048,925
1985–86	75.83	3,303,155	17.64	768,398	24.23	1,055,459
1986–87	91.11	3,968,752	27.84	1,212,710	27.70	1,206,612
1987–88	88.03	3,834,587	27.83	1,212,275	25.21	1,098,148
1988–89	104.73	4,562,039	23.98	1,044,569	32.69	1,423,976
1989–90	101.20	4,408,272	24.71	1,076,368	25.41	1,106,860
1990–91	108.74	4,736,714	27.40	1,193,544	30.00	1,306,800
1991–92	112.18	4,886,561	31.11	1,355,152	28.81	1,254,964
1992–93	109.90	4,787,244	32.00	1,393,920	27.78	1,210,097
1993–94	81.79	3,562,772	22.70	988,812	22.98	1,001,009
1994–95	109.12	4,753,267	26.49	1,153,904	30.20	1,315,512
1995–96	98.82	4,304,599	28.08	1,223,165	31.87	1,388,257
1996–97	100.31	4,369,504	29.04	1,264,982	31.89	1,389,128
1997–98	89.93	3,917,351	24.02	1,046,311	28.29	1,232,312
1998–99	99.89	4,351,208	21.72	946,123	27.94	1,217,066
1999–2000	92.08	4,011,005	14.43	628,571	23.05	1,004,058
200–01	70.41	3,067,060	12.55	546,678	19.93	868,151
201–02	66.37	2,891,077	11.89	517,928	18.90	823,284
2002–03	77.13	3,359,783	17.41	758,380	23.49	1,023,224
2003–04	89.40	3,894,264	22.57	983,149	25.86	1,126,462
2004–05	72.75	3,168,990	18.46	804,118	21.31	928,264
2005–06	96.82	4,217,479	23.17	1,009,285	25.14	1,095,098
2006–07	91.75	3,996,630	23.21	1,011,028	27.71	1,207,048
2007–08	87.79	3,824,132	17.69	770,576	20.60	897,336
2008–09	79.48	3,462,149	19.65	855,954	19.72	859,003
Average	89.83	3,913,095	22.66	987,160	25.60	1,115,201
Average (km^3/yr)		123,403		31,131		35,169
1 sigma		16,401		6097		5695

Source: Pakistan Commissioner for Indus Waters

Sutlej at Ferozpur

	30° 59′ 24.12″N	74° 33′ 17.00″E
Date	Discharge (m^3/s)	Discharge (ac ft/s)
28.9.1947	788,600	18.10
21.8.1948	238,875	5.48
18.8.1949	144,623	3.32
21.9.1950	353,936	8.13
25.8.1951	373,200	8.57
06.8.1952	278,900	6.40
06.8.1953	261,240	6.00
17.8.1954	283,920	6.52
07.10.1955	886,764	20.36
Average	401,118	9.21
km^3/yr	12,650	
1 sigma	8112	

Yamuna at Tajewala (above)

	30° 18′ 50.56″N	77° 35′ 08.10″E
Date	Discharge (m^3/s)	Discharge (ac ft/s)
25.9.1947	563,000	12.92
28.8.1948	135,834	3.12
31.7.1949	148,679	3.41
26.7.1950	129,246	2.97
22.8.1951	309,750	7.11
17.8.1952	131,380	3.02
12.8.1953	154,229	3.54
27.9.1954	252,550	5.80
04.10.1955	467,601	10.73
Average	254,697	5.85
km^3/yr	8032	
1 sigma	5107	1

Ravi at Mukesar (above Madhopur)

	32° 22′ 23.96″N	75° 36′ 21.72″E
Date	Discharge (m^3/s)	Discharge (ac ft/s)
26.9.1947	565,600	12.98
22.7.1948	79,218	1.82

Table 6 (*continued*)

Ravi at Mukesar (above Madhopur)

	32° 22′ 23.96″N	75° 36′ 21.72″E
Date	Discharge (m^3/s)	Discharge (ac ft/s)
05.8.1949	133,000	3.05
18.9.1950	301,000	6.91
29.7.1951	70,750	1.62
09.8.1952	101,000	2.32
03.8.1953	357,000	8.20
25.9.1954	152,481	3.50
05.10.1955	617,000	14.16
Average	264,117	5.20
km^3/yr	8329	
1 sigma	6627	

Beas at Deragopipur

	31° 52′ 31.64″N	76° 13′ 22.80″E
Date	Discharge (m^3/s)	Discharge (ac ft/s)
26.9.1947	278,000	6.38
19.8.1948	151,840	3.49
16.7.1949	200,350	4.60
25.7.1950	181,300	4.16
22.8.1951	479,750	11.01
03.8.1952	188,180	4.32
03.8.1953	207,750	4.77
19.8.1954	308,750	7.09
05.10.1955	298,500	6.85
Average	254,936	5.85
km^3/yr	8040	
1 sigma	3185	

Source: Irrigation and Power Research Institute Punjab, India

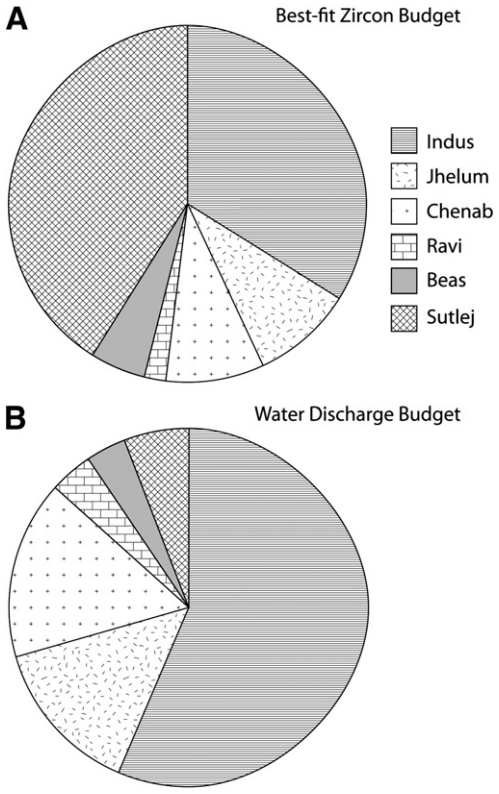

Fig. 12. Pie diagram showing (A) the relative contributions of the different tributaries to the total flux into the Indus delta based on zircon age populations and bulk sediment Nd isotopes providing a good match to the observed modern spectrum at Thatta, and (B) the relative pre-damming discharges from the rivers.

suggest that the composition of the sediments now at the delta reflects an earlier, likely Early-Mid Holocene, erosional state, while the water-based budget may be a better indicator of the present erosional regime.

Climate proxies indicate that the summer monsoon was much more intense in SW Asia during the Early Holocene (Enzel et al., 1999; Fleitmann et al., 2003) and this is known to influence erosion rates and patterns (Bookhagen et al., 2005; Clift et al., 2008a). The zircon budget at Thatta might imply that the Sutlej was much more sediment productive in the Early Holocene, assuming that each river then had the same zircon age population as it does today. Only the modern Sutlej appears to be rich enough in 1500–2300 Ma zircons to account for the abundance documented at Thatta. However, if climate and erosion patterns have changed since that time then even this premise may not be valid. It is possible that the Yamuna, which like the Sutlej is rich in 1250–2300 Ma grains, also used to contribute to the Indus, increasing these old zircons at Thatta and mimicking the effects of a higher Sutlej flux. Presently there is little other evidence to support this model. We can discount the possible influence of the Ghaggar in driving the change at the delta because this river is volumetrically small and does not contain a high proportion of 1500–2300 Ma zircons that are needed to drive the observed change. All we can say for sure is that the Lesser Himalaya delivered more sediment to the Indus system in the past than they do today, and that this is likely linked to monsoon weakening since 8 ka (Fleitmann et al., 2003) and lower amounts of landsliding in these ranges (Bookhagen et al., 2005). Mapping shows that the Lesser Himalaya were not glaciated at the Last Glacial Maximum (LGM) (Owen et al., 2002) and so changes in the extent of glaciation are not a factor causing this change.

An image of how erosion patterns have changed since the LGM can be derived by the division of the zircon populations into the four groupings defined above (0–300, 300–750, 750–1250 and 1500–2300 Ma). The sample at Thatta can be taken as representing Mid-Early Holocene erosion, while the modern erosion can be estimated using the water discharge budget. An impression of erosion at the LGM was derived by grouping existing measured zircon ages from LGM sediment cored at the Indus delta (Clift et al., 2008a). The results of this analysis are shown in Fig. 13. It is striking how dominant <300 Ma grains and therefore, erosion from the Karakoram and Transhimalaya, were at the LGM, while by the Early-Mid Holocene erosion of the Lesser Himalaya strengthened. The modern budget shows an increase in flux from Karakoram and reduced Lesser Himalayan erosion (Fig. 13). Since the Early Holocene the flux from the Lesser Himalaya has reduced, likely reflecting a weakening monsoon after 8 ka (Fleitmann et al., 2003; Gupta et al., 2003). Here we have shown that the Sutlej is the richest source of 1500–2300 Ma (Lesser Himalayan) zircons in the modern system, followed by the Jhelum (Figs. 1 and 11; Table 5). In the case of the Sutlej sample these grain could not be reworked from the Siwaliks because the sample was taken upstream of these rocks. We speculate that a stronger monsoon could have preferentially brought heavier rains to that part of the catchment and increased erosion there during the Early Holocene, as suggested by the evidence for landsliding at that time in that drainage (Bookhagen et al., 2006). Stronger Early Holocene erosion in the Siwaliks could also generate the change seen at the delta, assuming that the Indus basin Siwaliks are the same composition as those in Nepal.

6.10. Precipitation and erosion yield

Our sediment budget now allows us to examine whether tectonic forces or climate might be more important in controlling erosion rates within the Indus drainage. GPS surveys of the western Himalaya indicate that around half the convergence between India and Eurasia

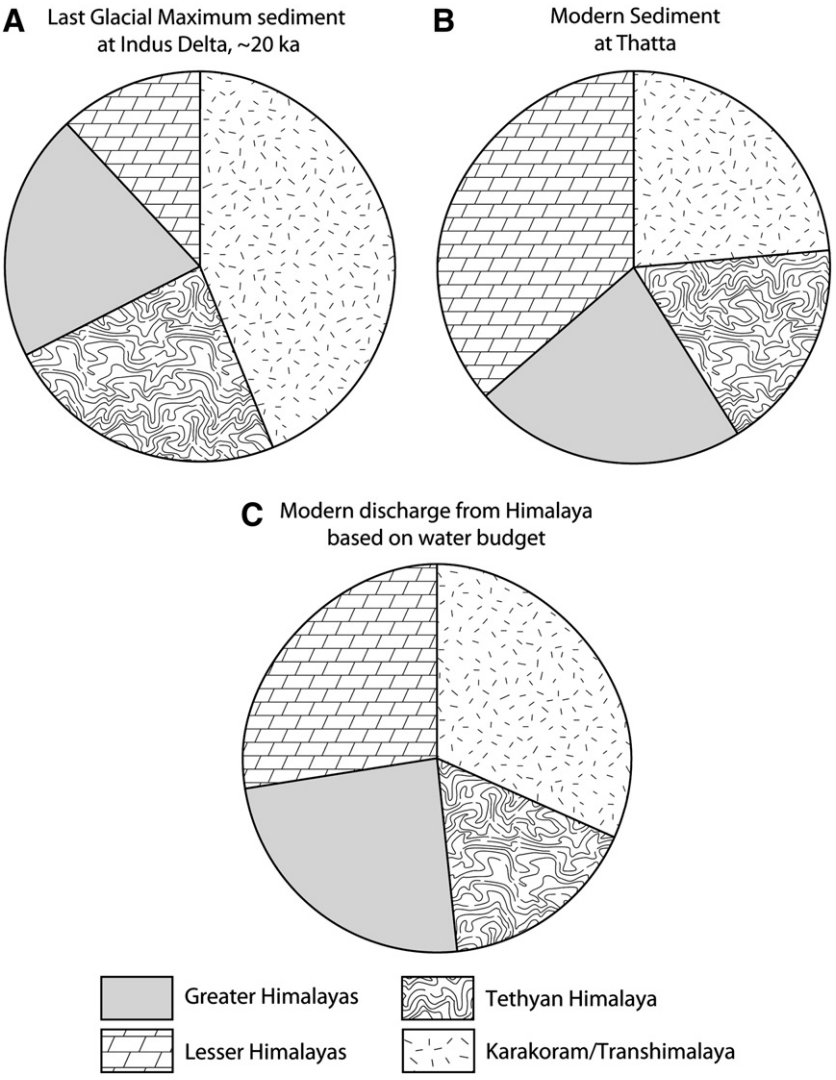

Fig. 13. Erosional budgets for the Indus River system based on zircon populations (A) ~20 ka sediment from the Indus Delta, representing sediment flux at the Last Glacial Maximum, (B) modern sediment at Thatta interpreted to reflect sediment flux in the early-mid Holocene, and (C) the calculated composition of sediment now being exported from the Himalaya.

is presently accommodated by shortening between the Main Frontal Thrust and the Indus Suture Zone (Jade et al., 2004), leading to significant rock uplift across the Himalayan front, with less deformation concentrated immediately to the north in Tibet. Certain key regions, such as Nanga Parbat, are locations of particularly rapid rock uplift that raise the possibility of faster erosion in those places (Zeitler et al., 1982). However, if the rapid rock uplift associated with the syntaxis and the metamorphic domes of the southern Karakoram was the primary control on erosion then we would expect these areas to be experiencing the fastest erosion and feeding large sediment volumes to the river. In this case the trunk up-stream Indus would be the greatest generator of sediment. However, our zircon-based sediment budget indicates that this part of the drainage contributed only around 35% of the total flux to the lower reaches during the earlier parts of Holocene, when the monsoon was strong. Discharge data now indicate that as much as 56% of the modern flux from the mountains is now from the upper Indus (Table 5). Moreover, Fig. 11 shows that most of that flux is from the Karakoram, rather than the more friable, low grade rocks of the Tethyan Himalaya, or from rapidly uplifting Nanga Parbat. Localized earthquakes do affect erosion patterns and rates but we argue that on the scale of a basin as large as the Indus that major changes in erosion patterns caused by earthquakes are unlikely to greatly affect the regional erosion patterns on timescales <10 ka. The effect that these events have is hard to constrain without a detailed Quaternary seismic record which does not yet exist. Here we discuss the potential links between the better defined climatic evolution and changes in erosion to see whether this might be a plausible mechanism.

What is driving rapid sedimentation production and transport in the Himalayan rivers? Fig. 2 shows the relationship between the major tributaries and the mean annual precipitation, as measured by NASA's Tropical Rainfall Measuring Mission (TRMM) (Bookhagen and Burbank, 2006). What is clear from this map is that the Himalayan front concentrates the rainfall, leaving Tibet, the Transhimalaya and the Karakoram in a rain shadow. Furthermore, rainfall decreases from a maximum between the Chenab and Beas Rivers of the Himalaya towards the NW, so that the upper Indus in particular is relatively dry. This overall regional trend in rainfall may be one of the primary controls on the supply of sediment into the lower Indus River because greater precipitation in the Chenab–Beas region may be driving the faster erosion and sediment supply compared to their neighbours (Table 5), at least at the present time. The wettest, Lesser Himalayan part of the Sutlej Valley is providing much more sediment to these rivers than would be expected from outcrop areas (Fig. 8). The same

might be said of the Jhelum, but the sample was taken downstream of the wide Siwalik exposure and this is an alternative source of the 1500–2300 Ma grains.

To better understand what is controlling the modern erosion we need to correct for the much greater length of the Sutlej and the Indus compared to the other river systems in order to estimate how sediment productive each river is. In this study we therefore measured the area of each river basin, but only consider those parts of the drainage north of the Main Frontal Thrust, i.e. in the mountains, not the flood plains, because on geological time scales these are the primary source of sediment, while deposition dominates in the flood plains. Estimates of sediment yield can be derived using both the zircon and water-based budgets (i.e., modern and Early Holocene), as shown in Table 7. We do this to compare differences in relative rather than absolute erosion rates, especially because if these estimates represent an earlier erosional state then the total sediment yield would have been higher than 250 Mt/yr, which was the pre-damming mass flux used for the modern water budget (Milliman and Syvitski, 1992). Sedimentation records from the delta show that the Early Holocene was a time of greatly enhanced sediment flux (Giosan et al., 2006), and so while the relative strengths of the different rivers would be meaningful the absolute values are not.

Sediment yield values can be calculated by dividing the total weight of sediment produced in each tributary by the area of the mountain drainage. The uncertainties in doing this are high because if the upper Indus now accounts for 56% of the total water discharge, and thus therefore supplies 56% of the 250 Mt/yr reaching the delta, then this would require 141 Mt/yr to have been supplied from the upper Indus to the delta prior to damming at Tarbela (Fig. 1). In practice however sedimentation in the reservoir behind the Tarbela dam indicates ~200 Mt/yr of supply to this point in the river (TAMS and HR Wallingford, 1998) (TAMS = Tippetts–Abbett–McCarthy–Stratton Consultants). Sediment and water gauging records at Attock Bridge indicate that the flux may even have been higher, with figures of 360 Mt/yr being recorded for the period 1868–1960 (TAMS, 1984). These higher values imply either than the river experiences major short-term changes in its carrying capacity, and/or that there is significant sediment storage between Tarbela and the delta, because the upper Indus flux alone exceeds the pre-damming sediment flux to the ocean estimated by Milliman and Syvitski (1992). The relative discharge from the upper Indus and the net 250 Mt/yr flux at the Indus delta would imply much lower volumes of sediment reaching the delta from the upper Indus than have reached the level of Tarbela Dam in the recent past.

All-India rainfall records show a strong 60-year cyclicity (Agnihotri et al., 2002), but the 1868–1960 sediment gauging record covers more than one of these cycles and should not be biased towards periods of stronger flux. Nonetheless, opportunities for sediment storage in central and northern Pakistan appear modest, because the river lies in an incised valley up to 20 m deep in these areas, implying recent erosion rather than sedimentation in the flood plains. The same is not true in southern Pakistan (Sindh Province) where some of the excess sediment may be stored, assuming that the different sediment flux studies are all accurate and not within error of each other. In order to assess the sediment-generating power of the sources we here consider only the net sediment flux to the Arabian Sea. We calculate yields from the upper Indus to the delta to be 741 t/yr km^2, using discharge as a proxy for carrying capacity. This number is somewhat less than the estimate of 1197 t/yr km^2 of Ali and De Boer (2007) for the Indus at Besham, located just north of Attock Bridge.

It is apparent that the yields in the upper Indus and Sutlej are lower than the other rivers (except the Beas), and this likely reflects the fact that these rivers both have large and mostly arid upper catchments that lie in the Himalayan rain shadow (Fig. 2). This is consistent with earlier sediment provenance work that demonstrated that erosion from the Transhimalaya, lying along the arid uppermost Indus, was not a major source to the river (Clift et al., 2002; Lee et al., 2003; Garzanti et al., 2005). This hypothesis is consistent with modern suspended sediment and water discharge budgets (Ali and De Boer, 2007). Sediment production in the upper Indus is largely limited to the Karakoram, and to a lesser extent the Transhimalaya and the Nanga Parbat Massif, as demonstrated by our U–Pb zircon ages and from the discharge records (Ali and De Boer, 2007) (Fig. 9). Estimating these terrains to cover ~60,000 km^2 we calculate that the effective yield would be 2347 t/yr km^2, using water discharge to calculate the erosional flux. This is comparable to values for several of the mountainous tributaries determined by gauging stations, which range up to 3373 t/yr km^2 (Ali and De Boer, 2007). These areas are not very wet compared to the Himalayan tributaries and demonstrate that a combination of glaciation and tectonics can be powerful erosion controls.

Nonetheless, the large-scale change in erosion patterns during the Holocene is consistent with what is expected from the waxing and waning of the monsoon over this same period, specifically in increasing and reducing rainfall in the Lesser Himalaya and Siwaliks. The solid Earth tectonic forces are stable over long periods of geological time (Molnar and Stock, 2009), and while uplift related to earthquakes can generate increased sediment flux locally, in a large basin like the Indus this effect is not expected to have a major impact on the composition of the river sediment on these timescales. If a disproportionate number of the large earthquakes since the LGM had been in the Sutlej Valley and then stopped after the Early Holocene then this could conceivably have caused the erosional changes seen at the delta. However, there is no record of Quaternary earthquakes and at the present time we consider this alternative less likely.

7. Conclusions

In this study we for the first time characterize the U–Pb age of zircon sand grains in all the major tributaries of the Indus River, as well as nearby neighbours in the Ghaggar and Yamuna Rivers. We further applied the same methodology to the bedrocks of the Sutlej in order to verify that detrital ages measured by LA-ICP-MS can be compared with bedrock values. Comparison of bedrock ages and sediments in the Sutlej Valley shows a close correspondence and a general consistency with earlier bedrock zircon ages. This study

Table 7
Estimates of sediment yield from Indus system rivers based on pre-damming sediment flux, both for total mountain drainage area and only those regions where precipitation exceeds 0.5 m/yr. Water budget is derived from data in Table 6.

River	Zircon-based yield (mt/yr)	Water-based yield (mt/yr)	Water discharge (km^3/yr)	Total mountain area (km^2)	Zircon-based yield (t/yr km^2)	Water-based yield (t/yr km^2)
Indus upstream	85.0	140.9	123.4	190,000	447	741
Jhelum	22.5	35.5	31.1	31,813	707	1116
Chenab	22.5	40.2	35.2	28,235	797	1423
Ravi	5.0	9.5	8.3	8223	608	1152
Sutlej	102.5	14.5	12.7	58,667	1747	247
Beas	12.5	9.1	8.0	13,914	898	656
Total Indus	250					

allows us to finger print the influence of each tributary on the drainage as a whole and constrain the age of the bedrocks in their catchment. We show that the upper Indus above Attock Bridge is dominated by grains younger than 200 Ma, quite different from any tributary to the east, but consistent with sources in the Karakoram, and to a lesser extent the Transhimalaya and Nanga Parbat. A rapid decrease in the abundance of young grains moving east indicates that the Indus has been stationary in the syntaxis over long periods of time. Sands in the Thar Desert show some similarities with the neighbouring Sutlej River, but a strong imprint of grains <200 Ma requires a dominant sediment transport from the lower reaches of the Indus, probably carried by the strong summer SW monsoon winds. Attempts to model the zircon age spectrum seen in the river at Thatta, near the delta, using recent water discharge data result in a poor match with the observed grain ages in that region. About 5000–10,000 yr is required to transport these grains from source to the delta, resulting in a mismatch between the modern discharge at the mountain front and the sediment zircon population close to the delta. We infer that the zircons close to the delta represent erosion during the Early-Mid Holocene, when discharge was much richer in 1500–2300 Ma zircons.

Erosion was stronger from the Lesser Himalaya in the Early Holocene, broadly correlating with the known monsoon maximum. We favour a dominant role for monsoon precipitation over solid Earth tectonic deformation in controlling changes erosion rates and sediment supply because although the upstream trunk Indus now accounts for ~56% of the sediment load, this shrank to only 35% in the Early Holocene when the summer monsoon was strong. At this time flux from the Sutlej, and/or an isotopically similar tributary, probably the Yamuna, formed the greatest contributor (41%). While we cannot rule out the influence of earthquakes in changing erosion patterns since the LGM the coherency of the changes in zircon populations seen at the delta with climate change are consistent with this being the primary control. While the zircons in the Indus, Chenab and Ravi are broadly consistent with relative extents of bedrock in their upper reaches the Sutlej shows preferential erosion of the Lesser Himalaya compared to other parts of the system. A similar situation affects the Lesser Himalaya and Siwaliks in the Jhelum River. This may reflect the heavier precipitation along the topographic break defined by the range front.

Supplementary materials related to this article can be found online at doi:10.1016/j.gloplacha.2010.11.008.

Acknowledgements

We thank Bodo Bookhagen for his help with regional rainfall data. Sanjeev Gupta (Imperial College) and Rajiv Sinha (IIT) contributed crucial sample material to this study. This work was funded by the Leverhulme Trust. The paper was improved thanks to the comments of two careful, anonymous reviewers.

References

Abanda, P.A., Hannigan, R.E., 2006. Effects of diagenesis on trace element partitioning in shales. Chem. Geol. 42–59.
Agnihotri, R., Dutta, K., Bhushan, R., Somayajulu, B.L.K., 2002. Evidence for solar forcing on the Indian monsoon during the last millennium. Earth Planet. Sci. Lett. 198, 521–527.
Algeo, T.J., Hannigan, R., Rowe, H., Brookfield, M., Baud, A., Krystyn, L., Ellwood, B.B., 2007. Sequencing events across the Permian–Triassic boundary, Guyrul Ravine (Kashmir, India). Palaeogeogr. Palaeoclimatol. Palaeoecol. 252, 328–346.
Ali, K.F., De Boer, D.H., 2007. Spatial patterns and variation of suspended sediment yield in the upper Indus River basin, northern Pakistan. J. Hydrol. 334, 368–387. doi:10.1016/j.jhydrol.2006.10.013.
Ali, K.F., De Boer, D.H., 2008. Factors controlling specific sediment yield in the upper Indus River basin, northern Pakistan. Hydrol. Processes 22, 3102–3114.
Amidon, W.H., Burbank, D.W., Gehrels, G.E., 2005a. Construction of detrital mineral populations: insights from mixing of U–Pb zircon ages in Himalayan rivers. Basin Res. 17 (4), 463–485.
Amidon, W.H., Burbank, D.W., Gehrels, G.E., 2005b. U–Pb zircon ages as a sediment mixing tracer in the Nepal Himalaya. Earth Planet. Sci. Lett. 235 (1–2), 244–260.
Anders, E., Grevesse, N., 1989. Abundances of the elements: meteoric and solar. Geochim. Cosmochim. Acta 53, 197–214.
Bayon, G., German, C.R., Boella, R.M., Milton, J.A., Taylor, R.N., Nesbitt, R.W., 2002. An improved method for extracting marine sediments fractions and its application to Sr and Nd isotopic analysis. Chem. Geol. 187, 179–199.
Bernet, M., van der Beek, P., Pik, R., Huyghe, P., Mugnier, J.-L., Labrin, E., Szulc, A.G., 2006. Miocene to Recent exhumation of the central Himalaya determined from combined detrital zircon fission-track and U/Pb analysis of Siwalik sediments, western Nepal. Basin Res. 18, 393–412. doi:10.1111/j.1365-2117.2006.00303.
Bookhagen, B., Burbank, D.W., 2006. Topography, relief, and TRMM-derived rainfall variations along the Himalaya. Geophys. Res. Lett. 33 (L08405). doi:10.1029/2006GL026037.
Bookhagen, B., Fleitmann, D., Nishiizumi, K., Strecker, M.R., Thiede, R.C., 2006. Holocene monsoonal dynamics and fluvial terrace formation in the northwest Himalaya, India. Geology 34 (7), 601–604.
Bookhagen, B., Thiede, R.C., Strecker, M.R., 2005. Late Quaternary intensified monsoon phases control landscape evolution in the northwest Himalaya. Geology 33 (2), 149–152.
Burbank, D.W., Beck, R.A., Mulder, T., 1996. The Himalayan foreland basin. In: Yin, A., Harrison, T.M. (Eds.), The Tectonics of Asia. Cambridge University Press, New York, pp. 149–188.
Campbell, I.H., Reiners, P.W., Allen, C.M., Nicolescu, S., Upadhyay, R., 2005. He–Pb double dating of detrital zircons from the Ganges and Indus rivers; implication for quantifying sediment recycling and provenance studies. Earth Planet. Sci. Lett. 237 (3–4), 402–432.
Carter, A., Bristow, C.S., 2001. Detrital zircon geochronology: enhancing the quality of sedimentary source information through improved methodology and combined U–Pb and fission-track techniques. Basin Res. 12 (1), 47–57. doi:10.1046/j.1365-2117.2000.00112.
Clift, P., Giosan, L., Blusztajn, J., et al., 2008a. Holocene erosion of the Lesser Himalaya triggered by intensified summer monsoon. Geology 36 (1), 79–82. doi:10.1130/G24315A.1.
Clift, P.D., Blusztajn, J.S., 2005. Reorganization of the western Himalayan river system after five million years ago. Nature 438 (7070), 1001–1003.
Clift, P.D., Campbell, I.H., Pringle, M.S., Carter, A., Zhang, X., Hodges, K.V., Khan, A.A., Allen, C.M., 2004. Thermochronology of the modern Indus River bedload; new insight into the control on the marine stratigraphic record. Tectonics 23 (TC5013). doi:10.1029/2003TC001559.
Clift, P.D., Giosan, L., Carter, A., et al., 2010. Monsoon control over erosion patterns in the Western Himalaya: possible feed-backs into the tectonic evolution. In: Clift, P.D., Tada, R., Zheng, H. (Eds.), Monsoon Evolution and Tectonic-Climate Linkage in Asia. Special Publication, 342. Geological Society, London, pp. 181–213.
Clift, P.D., Hoang, V.L., Hinton, R., Ellam, R., Hannigan, R., Tan, M.T., Nguyen, D.A., 2008b. Evolving East Asian river systems reconstructed by trace element and Pb and Nd isotope variations in modern and ancient Red River-Song Hong sediments. Geochem. Geophys. Geosyst. 9 (Q04039). doi:10.1029/2007GC001867.
Clift, P.D., Lee, J.I., Hildebrand, P., Shimizu, N., Layne, G.D., Blusztajn, J., Blum, J.D., Garzanti, E., Khan, A.A., 2002. Nd and Pb isotope variability in the Indus River system; implications for sediment provenance and crustal heterogeneity in the western Himalaya. Earth Planet. Sci. Lett. 200 (1–2), 91–106.
Clift, P.D., Plumb, R.A., 2008. The Asian Monsoon: Causes, History and Effects. Cambridge University Press, Cambridge. 288 pp.
DeCelles, P.G., Gehrels, G.E., Najman, Y., Martin, A.J., Carter, A., Garzanti, E., 2004. Detrital geochronology and geochemistry of Cretaceous–Early Miocene strata of Nepal: implications for timing and diachroneity of initial Himalayan orogenesis. Earth Planet. Sci. Lett. 227 (3–4), 313–330.
DeCelles, P.G., Gehrels, G.E., Quade, J., LaReau, B., Spurlin, M., 2000. Tectonic implications of U–Pb zircon ages of the Himalayan orogenic belt in Nepal. Science 288 (5465), 497–499.
DeCelles, P.G., Gehrels, G.E., Quade, J., Ojha, T.P., Kapp, P.A., Upreti, B.N., 1998. Neogene foreland basin deposits, erosional unroofing, and the kinematic history of the Himalayan fold-thrust belt, western Nepal. Geol. Soc. Am. Bull. 110 (1), 2–21.
Dunlap, W.J., Wysoczanski, R., 2002. Thermal evidence for Early Cretaceous metamorphism in the Shyok suture zone and age of the Khardung volcanic rocks, Ladakh, India. J. Asian Earth Sci. 20 (5), 481–490.
Enzel, Y., Ely, L.L., Mishra, S., Ramesh, R., Amit, R., Lazar, B., Rajaguru, S.N., Baker, V.R., Sandle, A., 1999. High-resolution Holocene environmental changes in the Thar Desert, northwestern India. Science 284, 125–128.
Fleitmann, D., Burns, S.J., Mudelsee, M., Neff, U., Kramers, J., Mangini, A., Matter, A., 2003. Holocene forcing of the Indian monsoon recorded in a stalagmite from southern Oman. Science 300 (5626), 1737–1739.
Fraser, J.E., Searle, M.P., Parrish, R.R., Noble, S.R., 2001. Chronology of deformation, metamorphism, and magmatism in the southern Karakoram Mountains. Geol. Soc. Am. Bull. 113 (11), 1443–1455.
Garzanti, E., Vezzoli, G., Ando, S., France-Lanord, C., Singh, S.K., Foster, G., 2004. Sand petrology and focused erosion in collision orogens: the Brahmaputra case. Earth Planet. Sci. Lett. 220 (1–2), 157–174.
Garzanti, E., Vezzoli, G., Ando, S., Paparella, P., Clift, P.D., 2005. Petrology of Indus River sands; a key to interpret erosion history of the western Himalayan syntaxis. Earth Planet. Sci. Lett. 229 (3–4), 287–302.
Ghose, B., Kar, A., Husain, Z., 1979. The lost courses of the Saraswati River in the Great Indian Desert; new evidence from Landsat imagery. Geog. J. 145 (3), 446–451.
Giosan, L., Clift, P.D., Blusztajn, J., Tabrez, A., Constantinescu, S., Filip, F., 2006. On the control of climate- and human-modulated fluvial sediment delivery on river delta development: the Indus. EOS Trans. Am. Geophys. Union 87 (52), OS14A-04.
Glennie, K.W., Singhvi, A.K., Lancaster, N., Teller, J.T., 2002. Quaternary climatic changes over Southern Arabia and the Thar Desert, India. In: Clift, P.D., Kroon, D., Gaedicke, C.,

Craig, J. (Eds.), The Tectonic and Climatic Evolution of the Arabian Sea Region. Special Publications, 195. Geological Society, London, pp. 301–316.
Gupta, A.K., Anderson, D.M., Overpeck, J.T., 2003. Abrupt changes in the Asian southwest monsoon during the Holocene and their links to the North Atlantic Ocean. Nature 421, 354–356.
Hodges, K., 2003. Geochronology and thermochronology in orogenic systems. In: Rudnick, R. (Ed.), The Crust. Elsevier-Science, Amsterdam, pp. 263–292.
Honegger, K., Dietrich, V., Frank, W., Gansser, A., Thoni, M., Trommsdorf, V.F., 1982. Magmatism and metamorphism in the Ladakh Himalayas (the Indus-Tsangpo suture zone). Earth Planet. Sci. Lett. 60, 178–194.
Jade, S., Bhatt, B.C., Yang, Z., Bendick, R., Gaur, V.K., Molnar, P., Anand, M.B., Kumar, D., 2004. GPS measurements from the Ladakh Himalaya, India: preliminary tests of plate-like or continuous deformation in Tibet. Geol. Soc. Am. Bull. 116, 1385–1391. doi:10.1130/B25357.1.
Kao, S.J., Milliman, J.D., 2008. Water and sediment discharge from small mountainous rivers, Taiwan: the roles of lithology, episodic events, and human activities. J. Geol. 116, 431–448. doi:10.1086/590921.
Krol, M.A., Zeitler, P.K., Copeland, P., 1996. Episodic unroofing of the Kohistan Batholith, Pakistan: implications from K-feldspar thermochronology. J. Geophys. Res. 101 (B12), 28149–28164.
Lavé, J., Avouac, J.P., 2001. Fluvial incision and tectonic uplift across the Himalaya of central Nepal. J. Geophys. Res. 106, 26,561–26,592. doi:10.1029/2001JB000359.
Le Fort, P., Debon, F., Sonet, J., 1983. Petrography, geochemistry and geochronology of some samples from the Karakoram Batholith (N. Pakistan). In: Shams, F.A. (Ed.), Granites of the Himalayas. Karakoram and Hindu Kush, Punjab University, Lahore, Pakistan, pp. 377–387.
Lee, J.I., Clift, P.D., Layne, G., Blum, J., Khan, A.A., 2003. Sediment flux in the modern Indus River traced by the trace element composition of detrital amphibole grains. Sed. Geol. 160, 243–257.
Ludwig, K., 2003. Isoplot 3.0. Special Publication. Geochronology Center, Berkeley, p. 4.
Métivier, F., Gaudemer, Y., 1999. Stability of output fluxes of large rivers in South and East Asia during the last 2 million years; implications of floodplain processes. Basin Res. 11 (4), 293–303.
Milliman, J.D., 1997. Fluvial sediment discharge to the sea and the importance of regional tectonics. In: Ruddiman, W.F. (Ed.), Tectonic Uplift and Climate Change. Plenum Press, New York, pp. 239–257.
Milliman, J.D., Syvitski, J.P.M., 1992. Geomorphic/tectonic control of sediment discharge to the ocean; the importance of small mountainous rivers. J. Geol. 100, 525–544.
Molnar, P., 2001. Climate change, flooding in arid environments, and erosion rates. Geology 29 (12), 1071–1074.
Molnar, P., Stock, J.M., 2009. Slowing of India's convergence with Eurasia since 20 Ma and its implications for Tibetan mantle dynamics. Tectonics 28(TC3001). doi:10.1029/2008TC002271.
Murray, R.W., Leinen, M., 1993. Chemical transport to the seafloor of the equatorial Pacific Ocean across a latitudinal transect at 135o256 W: tracking sedimentary major, trace, and rare earth element fluxes at the equator and the Intertropical Convergence Zone. Geochim. Cosmochim. Acta 57, 414–4163.
Nesbitt, H.W., Young, G.M., 1982. Early Proterozoic climates and plate motions inferred from major element chemistry of lutites. Nature 299 (5885), 715–717.
Owen, L.A., Finkel, R.C., Caffee, M.W., 2002. A note on the extent of glaciation throughout the Himalaya during the global last glacial maximum. Quat. Sci. Rev. 21 (1–3), 147–157.
Parrish, R.R., Tirrul, R., 1989. U–Pb age of the Baltoro Granite, Northwest Himalaya, and implications for monazite U–Pb systematics. Geology 17, 1076–1079.
Pearce, N.J.G., Perkins, W.T., Westgate, J.A., Gorton, M.P., Jackson, S.E., Neal, C.R., Chenery, S.P., 1997. A compilation of new and published major and trace element data for NIST SRM 610 and NIST SRM 612 glass reference materials. Geostand. News 21 (1), 115–144.
Ravikant, V., Wu, F.Y., Ji, W.Q., 2009. Zircon U–Pb and Hf isotopic constraints on petrogenesis of the Cretaceous–Tertiary granites in eastern Karakoram and Ladakh, India. Lithos 110, 153–166.
Robinson, R.A.J., Bird, M.I., Oo, N.W., et al., 2007. The Irrawaddy River sediment flux to the Indian Ocean: the original nineteenth-century data revisited. J. Geol. 115 (6), 629–640.
Rudnick, R.L., Fountain, D.M., 1995. Nature and composition of the continental crust; a lower crustal perspective. Rev. Geophys. 33, 267–309.
Ruhl, K.W., Hodges, K.V., 2005. The use of detrital mineral cooling ages to evaluate steady state assumptions in active orogens: an example from the central Nepalese Himalaya. Tectonics 24 (4), TC4015. doi:10.1029/2004TC001712.
Saini, H.S., Tandon, S.K., Mujtaba, S.A.I., Pant, N.C., Khorana, R.K., 2009. Reconstruction of buried channel-floodplain systems of the northwestern Haryana Plains and their relation to the 'Vedic' Saraswati. Curr. Sci. 97 (11), 1634–1643.
Schärer, U., Copeland, P., Harrison, T.M., Searle, M.P., 1990. Age, cooling history, and origin of post-collisional leucogranites in the Karakoram Batholith; a multi-system isotope study. J. Geol. 98 (2), 233–251.
Schärer, U., Xu, R.-H., Allègre, C.J., 1984. U–Pb geochronology of Gangdese (Transhimalaya) plutonism in the Lhasa-Xigaze region, Tibet. Earth Planet. Sci. Lett. 69 (2), 311–320.
Singh, S., Kumar, R., Barley, M.E., Jain, A.K., 2007. SHRIMP U–Pb ages and depth of emplacement of Ladakh batholith, eastern Ladakh. Indian J. Asian Earth Sci. 30 (3), 490–503.
Singh, S.K., Sarin, M.M., France-Lanord, C., 2005. Chemical erosion in the eastern Himalaya; major ion composition of the Brahmaputra and d13C of dissolved inorganic carbon. Geochim. Cosmochim. Acta 69 (14), 3573–3588.
Singhvi, A.K., Williams, M.A.J., Rajaguru, S.N., et al., 2010. A 200 ka record of climatic change and dune activity in the Thar Desert. Indian Quat. Sci. Rev. doi:10.1016/j.quascirev. 2010.08.003.
Sláma, J., Košler, J., Condon, D.J., et al., 2008. Plezovice zircon A new natural reference material for U–Pb and Hf isotopic microanalysis. Chem. Geol. 249, 1–35. doi:10.1016/j.chemgeo.2007.11.005.
Smith, J.P., 2007. Short-to-medium term sediment accumulation in low-energy subtidal areas of the lower Hudson River estuary: geochemical tracers and applications. Ph.D. Thesis, University of Massachusetts, Boston, 212 pp
Subramanian, V., 1996. The sediment load of Indian rivers — an update. Erosion and Sediment Yield: Global and Regional Perspectives. Special Publication, 236. International Association of Hydrological Sciences, pp. 183–189.
Syvitski, J.P.M., 2003. Supply and flux of sediment along hydrological pathways: research for the 21st century. Global Planet. Change 39 (1–2), 1–11.
TAMS, 1984. Tarbela Dam Project: Completion Report on Design and Construction. WAPDA, Lahore.
TAMS, HR Wallingford, 1998. Tarbela Dam Sediment Management Study. WAPDA, Lahore.
Thomas, J.V., Kar, A., Kailath, A.J., Juyal, N., Rajaguru, S.N., Singhvi, A.K., 1999. Late Pleistocene–Holocene history of eolian accumulation in the Thar Desert, India. Z. Geomorphol 116, 181–194 N.F., Suppl. Bd.
Tripathi, J.K., Bock, B., Rajamani, V., Eisenhauer, A., 2004. Is River Ghaggur, Saraswati? Geochemical constraints. Curr. Sci. 87 (8), 1141–1145.
Valdiya, K.S., 1980. Geology of the Kumaon Lesser Himalaya. Wadia Institute of Himalayan Geology, Dehra Dun. 291 pp.
Vannay, J.-C., Grasemann, B., Rahn, M., Frank, W., Carter, A., Baudraz, V., Cosca, M., 2004. Miocene to Holocene exhumation of metamorphic crustal wedges in the NW Himalaya; evidence for tectonic extrusion coupled to fluvial erosion. Tectonics 23, TC1014. doi:10.1029/2002TC001429.
Wasson, R.J., 2003. A sediment budget for the Ganga–Brahmaputra catchment. Curr. Sci. 84 (3), 1041–1047.
Weinberg, R.F., Dunlap, W.J., 2000. Growth and deformation of the Ladakh Batholith, northwest Himalayas: implications for timing of continental collision and origin of calc-alkaline batholiths. J. Geol. 108, 303–320. doi:10.1086/314405.
Whipple, K.X., 2001. Fluvial landscape response time: how plausible is steady-state denudation? Amer. J. Sci. 301, 313–325.
Wu, F.Y., Clift, P.D., Yang, J.H., 2007. Zircon Hf isotopic constraints on the sources of the Indus Molasse, Ladakh Himalaya, India. Tectonics 26, TC2014. doi:10.1029/2006TC002051.
Xie, P., Arkin, P.A., 1997. Global precipitation: a 17-year monthly analysis based on gauge observations, satellite estimates and numerical model outputs. Bull. Am. Meteorol. Soc. 78, 2539–2558.
Zeilinger, G., Burg, J.P., Schaltegger, U., Seward, D., 2001. New U/Pb and fission track ages and their implication for the tectonic history of the lower Kohistan Arc Complex, northern Pakistan. J. Asian Earth Sci. 19 (3 S), 79–81.
Zeitler, P.K., 1985. Cooling history of the NW Himalaya, Pakistan. Tectonics 4 (1), 127–151.
Zeitler, P.K., Chamberlain, C.P., 1991. Petrogenetic and tectonic significance of young leukogranites from the northwestern Himalaya, Pakistan. Tectonics 10 (4), 729–741.
Zeitler, P.K., Chamberlain, C.P., Smith, H.A., 1993. Synchronous anatexis, metamorphism, and rapid denudation at Nanga-Parbat (Pakistan Himalaya). Geology 21 (4), 347–350.
Zeitler, P.K., Johnson, N.M., Naeser, C.W., Tahirkheli, R.A.K., 1982. Fission-track evidence for Quaternary uplift of the Nanga Parbat region, Pakistan. Nature 298 (5871), 255–257.